



Faculty of Science and Technology

MASTER'S THESIS

Study program/ Specialization: Master of Science in Petroleum Technology/ Well Engineering	Spring semester, 2014 Open
Writer: Segun Gideon Aiyeru (Writer's signature)
Faculty supervisor: Professor Bernt S. Aadnøy	
Title of thesis: 'Inversion methods to determine the in-situ stresses'	
Credits (ECTS): 30	
Key words: -In-situ stress -LOT -Inversion -Overburden, Horizontal stresses -Azimuth	Pages: 83 + enclosures: 3 Matlab files 1 Excel file Stavanger, 12th June, 2014.

Dedication

This thesis is dedicated to my beautiful and lovely wife, Rimini Machunga-Aiyeru who gave me full permission, encouragement and support to pursue my dream and stood by me for these past years.

Acknowledgement

First and foremost, I give thanks to the Almighty God who gave me the wisdom and strength to successfully complete my studies.

My profound appreciation goes to my supervisor, Professor Bernt S. Aadnøy for his tutelage, inspiration and guidance throughout my studies and particularly during my thesis.

I would like to thank Jóannes Djurhuus of Statoil for his invaluable assistance in helping to decode the model and in the preparation of my program.

I would also like to thank Mesfin Agonafir Belayneh for his constant encouragement and willingness to always be of help.

Abstract

The challenges pose by the uncertainty in the in-situ stress measurement in the petroleum and mining industries are enormous. A handy computer tool to estimate the magnitude and direction of the horizontal in-situ stresses is developed in this thesis. The tool is based on the mathematical model proposed by Bernt S. Aadnøy which makes use of data from hydraulic fracture test to back calculate to obtain the horizontal principal in-situ stresses. To demonstrate the reliability of the program it was applied to real fracture data from wells in the North Sea. Two field cases were considered. The first field case illustrated the ability of the programming tool to accurately estimate the state of stress of the formation and also verify the validity of the results by computing the estimated formation fracture pressure to be compared with the measured data from LOT. The second field case exhibited the tool's ability to predict the fracture pressure of a future well to be drilled. The results obtained showed excellent correlations with tests data.

Table of Contents

Dedication	ii
Acknowledgement	iii
Abstract	iv
Table of Contents	v
List of Tables	viii
List of Figures	ix
Nomenclature	x
1.0 Introduction.....	1
1.1 Background	1
1.2 Objective	4
2.0 Literature Research	5
2.1 Introduction	5
2.2 Stress	5
2.3 Strain	6
2.4 Hooke's law.....	6
2.5 Poisson's ratio	7
2.6 Components of stress	7
2.7 In-situ stress.....	8
2.8 Overburden stress.....	9
2.9 Horizontal stresses.....	10
2.10 Principal stresses	10
2.11 Methods to Measure Stress	12
2.12 Formation pore pressure.....	13
2.13 Effective stress	14

2.14	State of stress.....	15
2.15	Effect of Faulting on in-situ stresses	16
2.16	In-situ stresses Bounds	17
2.17	Distribution of Stresses around a wellbore	18
2.18	Stress analysis equations	20
2.18.1	Equations of equilibrium.....	20
2.18.2	Compatibility equations	22
2.18.3	Constitutive relations	23
2.18.4	Boundary condition.....	24
2.18.5	Stress transformation and equations	25
3.0	Failure Models and Criteria	27
3.1	Failure Criteria	27
3.1.1	The Von Mises Failure Model	27
3.1.2	Mohr-Coulomb Failure Criterion.....	29
3.1.3	The Griffith Failure Criterion	30
3.1.4	Hoek-Brown Failure Criterion	31
3.1.5	The Drucker-Prager Failure Criterion.....	31
3.1.6	The Mogi-Coulomb Failure Criterion.....	32
3.2	Mechanisms of Failure	33
3.3	Wellbore Collapse	33
3.4	Wellbore Fracture.....	34
3.5	Fracture gradient	34
3.5.1	Experimental or direct method.....	34
3.5.2	Theoretical or indirect method.....	36
4.0	Fracture Model.....	39

In-Situ stress measurement from LOT data using Inversion method

4.1	Inversion Technique.....	39
4.2	Other models used.....	46
5.0	Computer Data Program	50
5.1	Introduction	50
5.2	Modelling	50
5.3	Quality Check.....	51
5.4	Prognosis	51
5.5	User guide	51
6.0	Field cases, simulation and discussion of results.....	55
7.0	Summary and Conclusion	65
	References.....	66
	Appendix.....	68

List of Tables

Table 2-1: Sign Convention for rocks and other engineering materials.	5
Table 2-2: Technology for the prediction of tophole formation pore pressures. (Peuchen and Klein, 2011)	14
Table 3: In-situ stresses general bounds for Normal, Strike-slip and Reverse Faults.	18
Table 4: Fracturing data for Field case 1	55
Table 5: Comparison of the measured and estimated fracture pressure of Case 1, Simulation 1.	57
Table 6: Comparison of the measured and estimated fracture pressure of Case 1, simulation 2.	58
Table 7: Comparison of the measured and estimated fracture pressure of Case 1, simulation 3.	59
Table 8: Comparison of the measured and estimated fracture pressure of Snorre field	60
Table 9: Fracturing data for Field case 2	62
Table 10: Comparison of the measured and estimated fracture pressure of Case 2, simulation 1	63
Table 11: Comparison of the measured and estimated fracture pressure of Case 2, simulation 2	64

List of Figures

Figure 1-1: Drilling Window (Nguyen, 2013).....	2
Figure 2-1: Stress state of a cube represented in three dimensions	7
Figure 2-2 Orientation of In-situ stresses in a rock formation.....	8
Figure 2-3 Principal In-situ stresses in a vertical borehole.....	11
Figure 2-4: Fault types and associated stresses. (FJÆR et al., 2008)	17
Figure 2-5: Plots of Collapse and Fracture pressure against wellbore inclination (Aadnøy et al., 2013)	17
Figure 2-6: A schematic showing in-situ stresses around a wellbore (Aadnøy and Looyeh, 2011).	19
Figure 2-7: (a) Rock formation with uniform stress state, (b) Rock formation with a drilled hole where the stress state will change. (Aadnøy and Looyeh, 2011).....	20
Figure 2-8: Stresses position around a borehole. (Aadnøy and Looyeh, 2011).....	21
Figure 3-1 Von Mises failure envelope from triaxial test data (Aadnøy and Looyeh, 2011).....	28
Figure 3-2 Mohr-Coulomb failure envelope from triaxial test data (Aadnøy and Looyeh, 2011).....	29
Figure 3-3 A test specimen Griffith criterion (Aadnøy and Looyeh, 2011)	30
Figure 3-4 Hoek-Brown failure model using triaxial test data (Aadnøy and Looyeh, 2011).....	31
Figure 3-5 Mogi-Coulomb failure envelope for Triaxial and polyaxial data (Aadnøy and Looyeh, 2011)	33
Figure 3-6: A plot showing the change in surface pressure during Extended Leak off test (Raaen et al., 2006)	36
Figure 4-1: Well Geometry.....	39
Figure 4-2: Fracture positions on wellbore wall.....	41
Figure 5-1: Data Capture Sheet.....	52
Figure 5-2: Graphic User Interface Layout.....	53
Figure 5-3: Graphic User Interface Results Output	54
Figure 6-1: In-situ stresses and error squared around the wellbore case 1, simulation 1.	56
Figure 6-2: In-situ stresses and error squared around the wellbore case 1, simulation 2	58
Figure 6-3: Horizontal view of well.....	61
Figure 6-4: Vertical view of well.....	61

Nomenclature

A	Surface area (m^2 , in^2)
F	Force (N, lbf)
σ	Normal stress (Pa, psi)
ε	Normal strain
τ	Shear stress (Pa, psi)
τ_o	Cohesive strength (Pa, psi)
γ	Wellbore inclination from vertical axis (degrees), Shear strain
φ	Geographical azimuth (degrees)
E	Young's modulus (Pa, psi)
ν	Poisson's ratio
\emptyset	Angle of internal friction (degrees), Porosity
g	Gravitational acceleration (ms^{-2} , fts^{-2})
G	Shear modulus (Pa, psi)
K	Bulk modulus, Constitutive relation parameter
I	Invariant
J	Deviatoric invariant
δ	Stability margin (Pa, psi)
α	Fracture parameter
β	Biot's constant, Fracture parameter, In-situ stress direction (degrees)
ρ_b	Formation bulk density (kgm^{-3} , $lb.in^{-3}$)

In-Situ stress measurement from LOT data using Inversion method

ρ_w	Density of water (kgm^{-3} , lb.in^{-3})
σ_t	Tensile stress (Pa, psi)
σ_v	Overburden stress (Pa, psi)
σ_H, σ_h	Maximum and minimum horizontal stresses (Pa, psi)
$\sigma_1, \sigma_2, \sigma_3$	Maximum, intermediate and minimum principal stresses (Pa, psi)
P_o	Pore pressure (Pa, psi)
P_w	Well pressure (Pa, psi)
P_{wc}	Well collapse pressure (Pa, psi)
P_{wf}	Well fracture pressure (Pa, psi)
r, θ, z	Cylindrical coordinate system
x, y, z	Cartesian coordinate system
u, v, w	Displacement in x, y and z directions (m, in)
LOT	Leak-off test
LOP	Leak-off pressure
FBP	Formation breakdown pressure
ISIP	Instantaneous shut-in pressure
FIT	Formation integrity test
FPP	Formation propagation pressure
FCP	Formation closure pressure
XLOT	Extended Leak-off test

1.0 Introduction

Borehole instability problems, maximum reservoir drainage and oriented perforation for sand control, are some of the major issues in the oil industry worldwide. In a study by Aadnøy et al. (2009) the petroleum industry spend huge sum of around 2 to 5 billion USD on issues related to borehole instability alone (Thorsen, 2011). To address this problem, the solution has been narrowed down to the ability to have much knowledge about properties of the rock formation before drilling. Important information such as; formation pore pressure, fracture gradient, well trajectory and bedding plane, formation reactiveness, and in-situ stresses are very key to a successful drilling operation. With advancement in technology, the formation pore pressure, well trajectory and bedding plane can be accurately estimated; the same cannot be said for the measurement of the in-situ stresses. The measurement of the in-situ stresses is usually not straightforward. The need for accurate measurement of the magnitude and direction of the formation in-situ stresses is becoming increasingly important because of the drilling of highly deviated, horizontal and deeper wells with complex configurations.

1.1 Background

To drill a hole successfully, the drilling mud must be maintained in the drilling window to achieve wellbore stability and avoid extreme cases of fracture or collapse. The drilling mud pressure must not exceed the minimum formation stress else, it may result in fracture of the formation. Likewise, if the drilling mud weight is less than the formation pore pressure, collapse may occur. Figure 1-1 shows a sketch of a drilling window. The main aim of a drilling engineer is to ensure that he stays within this window irrespective of how narrow the window gets. The formation stresses define the boundaries of this window. Together with other factors as listed above, the knowledge of in-situ stresses magnitude and orientation are critical to successful drilling operation, well completion, production and stimulation.

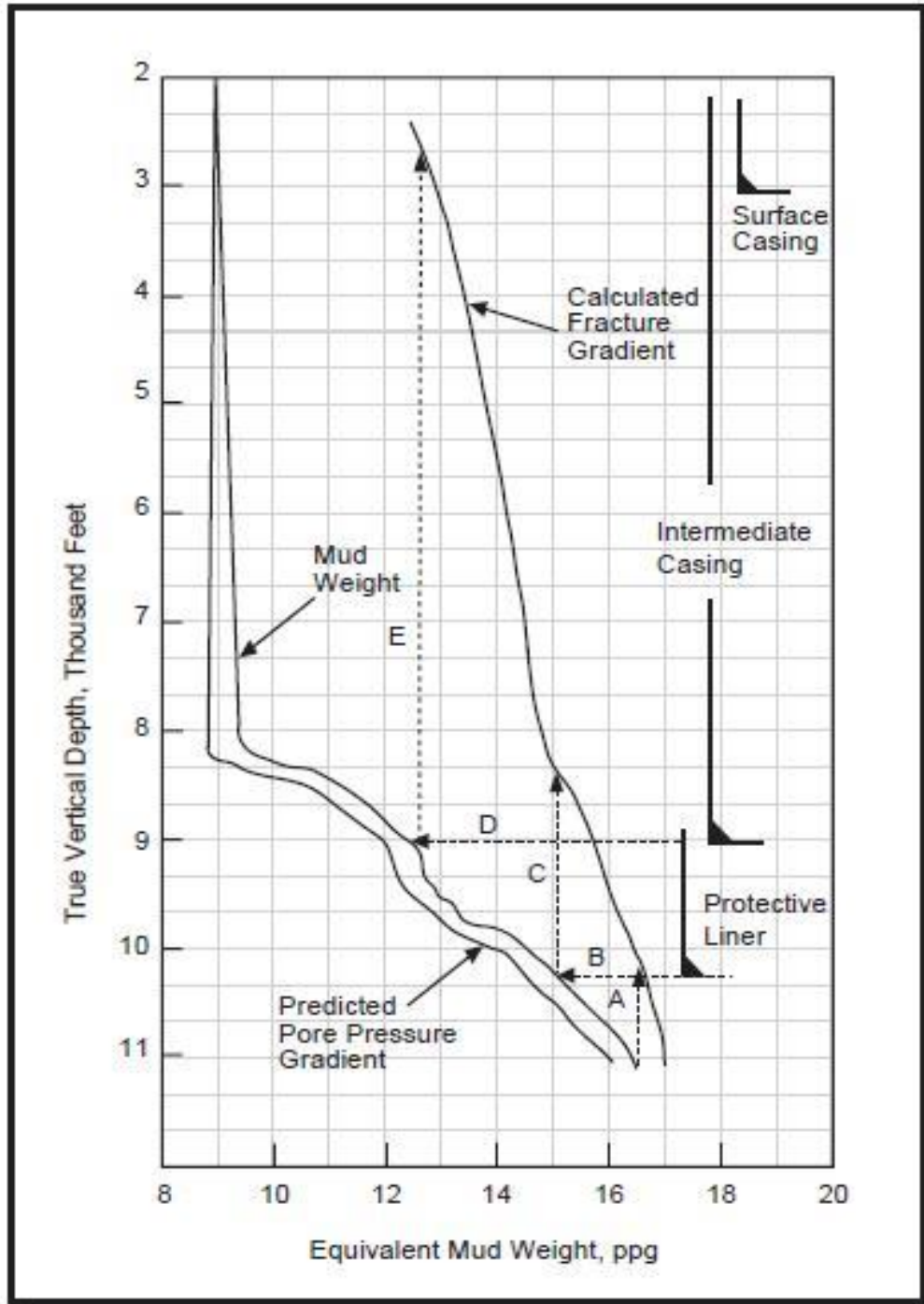


Figure 1-1: Drilling Window (Nguyen, 2013)

As highlighted by Aadnøy and Looyeh (2011), it is important to determine the in-situ stresses for the following reasons:

- Getting a basic knowledge of structure of the formation and position of anomalies, groundwater flows etc.
- Finding basic data on the formation stress state.
- Getting the orientation and magnitude of the major principal stresses.
- Finding the stress effects that may affect drilling and production processes.
- Discovering the directions that the formation rock is likely to break.
- Identifying the main boundary conditions to carry out a wellbore instability analysis.

The in-situ stresses are the overburden, minimum and maximum horizontal stresses. Based on the knowledge from mining and geotechnical industry, the in-situ stresses are ideally not homogenous, that is, not equal in magnitudes (Aadnoy, 1989). As difficult as it is to measure, fortunately, significant progress have been made in the measurement of in-situ principal stresses. It is generally accepted that the overburden is easily derived from logs. That left us with the challenge of accurately measuring the horizontal stresses. Unfortunately, there is no direct method to measure in-situ stresses. In the quest to accurately measure the horizontal in-situ stresses, some models have been developed. However, it is generally accepted that hydraulic fracturing is the most accurate method to measure stress at deep hole.

As shown by Aadnoy (1989), the magnitude and direction of the horizontal in-situ stresses can be estimated from leak-off data using inversion method. The method makes use of the fracture equation which is derived from the Kirsch equations and stress transformation equation to determine the horizontal stresses. It utilizes sets of data taken from different wells with different inclination and azimuth at the same location and solving to find the in-situ stresses. When tested on field data, the results were satisfactory.

In this thesis, focus is on the use of the linear elastic model developed by Bernt Aadnøy using inversion method.

1.2 Objective

This paper aims to simplify and make user friendly the model proposed by Aadnoy (1989) to determine horizontal in-situ stresses from Leak-off data. This would be achieved by developing a tool which is based on modern computer language that is easy to utilize and can help save valuable time during well planning and field development. The objective of the thesis would be achieved in the following steps:

1. Give basic Literatures relevant to the subject matter
2. Present mathematical models used for estimating in-situ stresses
3. Develop a MATLAB computer program to handle complex simulations.
4. Simulate field cases.

2.0 Literature Research

2.1 Introduction

This thesis begins with some background literature presenting fundamental concept necessary to comprehending the subject of study.

2.2 Stress

It is important to understand the concept of stress in general and in particular as it relates to rock mechanics.

Generally, stress is defined as the ratio of force to cross sectional unit area.

Mathematically,

$$\sigma = \frac{\text{Force}}{\text{Area}} = \frac{F}{A} \quad 2.1$$

Pascal (Pa, which is the same as N/m²) is the SI unit of stress, σ . Though, Pounds per square inch (psi) is commonly used in the oil and gas industry.

Stress is developed as a reaction or internal resistance in a body that is experiencing external forces or loadings. The area the force is acting on could be a surface or an imaginary plane. Stress is not dependent on the size and shape of a body but it is dependent on its orientation (Aadnøy and Looyeh, 2011). There are generally two types of stresses in a body; a stress that acts perpendicular to the plane, called normal stress, σ , and another stress called shear stress, τ , which acts parallel to the plane.

It is also of significant importance to note the differences in the sign convention when dealing with rock mechanics and other materials.

Table 2-1: Sign Convention for rocks and other engineering materials.

	Compressive Stresses	Tensile Stresses
Solid Rock	+	-
Other Engineering Materials	-	+

2.3 Strain

Since stress is a quantity that cannot be measured directly, the knowledge of strain is very key to the determination of stresses in engineering materials. The strain of a body or material is determined by applying load or force to the body and measuring the deformation or change in dimensions caused by the loading. The change in dimension divided by the original dimension gives the definition of a strain.

Mathematically,

$$\varepsilon = \frac{dl}{l_o} = \frac{l - l_o}{l_o} \quad 2.2$$

where ε is the strain, dl is the change in length, l_o is the original length and l is the new length.

For large deformations, the above equation 2.2 becomes invalid and appropriate equations were given by Almansi, equation 2.3 and Green, equation 2.4 (Aadnøy and Looyeh, 2011).

$$\varepsilon = \frac{l^2 - l_o^2}{2l^2} \quad 2.3$$

$$\varepsilon = \frac{l^2 - l_o^2}{2l_o^2} \quad 2.4$$

2.4 Hooke's law

The Hooke's law defines the stiffness of a material. It shows how the strain and the stress are related linearly and states that the ratio of the stress to strain of a material is a constant given by the Young's modulus, E. The Young's modulus which is also referred to as elastic modulus or E-modulus is given by the equation:

$$E = \frac{\sigma_x}{\varepsilon_x} \quad 2.5$$

Substituting equation 2.1 and equation 2.2 into equation 2.5 and re-arranging yields:

$$dl = \frac{F_x l_o}{EA} \quad 2.6$$

2.5 Poisson's ratio

The Poisson's ratio relates the lateral strain to axial strain in a material that is subject to load. It is given by the equation:

$$v = -\frac{\varepsilon_x}{\varepsilon_y} \quad 2.7$$

2.6 Components of stress

It is important to determine the stresses with respect to the orientation in the three perpendicular directions in order to get a vivid representation of the stress state at a point. σ_x , σ_y and σ_z are the normal stresses in the x, y and z plane respectively and the shear stresses are τ_{xy} , τ_{xz} , τ_{yx} , τ_{yz} , τ_{zx} and τ_{zy} in x, y and z planes as shown in Figure 2-1.

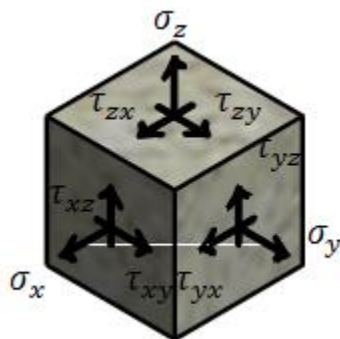


Figure 2-1: Stress state of a cube represented in three dimensions

A total of nine different stress components are identified and represented in the stress tensor as shown in equation 2.8

$$[\sigma] = \begin{bmatrix} \sigma_x & \tau_{xy} & \tau_{xz} \\ \tau_{yx} & \sigma_y & \tau_{yz} \\ \tau_{zx} & \tau_{zy} & \sigma_z \end{bmatrix} \quad 2.8$$

The subscripts in the shear stresses indicate the stress component direction and the axis perpendicular to the plane on which the stress acts. The stress tensor is symmetrical and assigning the first or second subscripts to direction or plane is a thing of choice as it plays no significant effect on the outcome (FJÆR et al., 2008).

2.7 In-situ stress

The in-situ stress, also known as far-field stress is the state of the stress of the rock formation in its original, relaxed and undisturbed position, that is, before any drilling activity is carried out. These stresses are generally compressive in nature. There are usually three In-situ principal stresses, mutually perpendicular to one another and existing at any point in the subsurface, as shown in Figure 2-2. They are the overburden, maximal and minimal horizontal stresses (Aadnøy and Looyeh, 2011). The vertical stress, which is also called overburden, may not necessarily be a principal stress due to the topography which might not be horizontal or due to some other geological processes, faults and tectonic stresses (Thorsen, 2011). In the following, we will try to look into these stresses in more details.

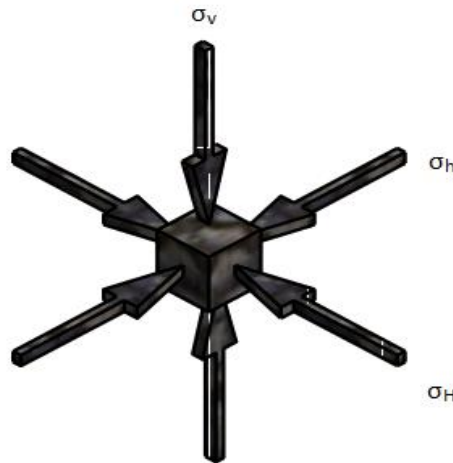


Figure 2-2 Orientation of In-situ stresses in a rock formation.

2.8 Overburden stress

The overburden stress which is also called the vertical stress is as a result of the weight of overlaying rock matrices and the fluids in the rock pores. Geological effects like salt dome or magma can also be sources of the overburden stress. Due to Poisson's ratio effect, the weight exerted by the vertical stress component usually has the tendency to stretch and widen the rocks underneath in the horizontal lateral direction (Aadnøy and Looyeh, 2011). The overburden stress can readily be calculated as shown below:

$$\sigma_v = \int_0^d \rho_b(h)gdh \quad 2.9$$

d = the depth of the rock formation (ft)

g = constant due to gravity (32.175ft/s²)

h = the vertical height of the formation (ft)

ρ_b = the bulk density of the formation (lb. /ft³)

All the parameters except the formation bulk density in the above equation can be gotten directly and at any depth.

The bulk density of the formation represents a total of the densities of the rock grain and pore fluid together with the formation rock porosity. Due to compaction caused by overlaying formation, the porosity decreases with depth and hence increase in formation bulk density. This relation is illustrated in the equation 2.10 used to determine the formation bulk density.

$$\rho_b = \rho_R (1 - \phi) + \rho_F \phi \quad 2.10$$

where ρ_R is the density of the rock grain, ρ_F is the density of the fluid contained in the pore and ϕ is the rock porosity.

With the determination of the average formation bulk density and knowledge of the pore pressure gradient, the overburden stress can be calculated at all depths by varying the depth term [d] in the equation given below:

$$\sigma_v = \rho_bgd \quad 2.11$$

2.9 Horizontal stresses

As discussed earlier, the effect of Poisson's ratio tends to expand the rock formation underneath. However, the lateral expansion is also been confined and pushed back by the adjoining rock materials. This result in the formation of horizontal stresses which are called, the maximum and minimum horizontal stresses (Aadnøy and Looyeh, 2011). Ideally, one would expect the two horizontal stresses to be equal but that is not often the case because of natural effects such as uneven topography or faults thereby resulting in uneven stresses. Because it is horizontal, natural phenomena like earthquake makes the stresses to undergo changes. In a relaxed lithology, the horizontal stresses are smaller in magnitude than the overburden stress. In subsequent chapter we will look at the advancement made in relation to measuring the horizontal stresses.

2.10 Principal stresses

The principal stresses serve as the maximum and minimum stresses in the formation. At the planes where the principal stresses act, all shear stresses become zero. Their magnitude and direction have significant effect on the failure of rocks during drilling operation. In an exceptional case, as shown in Figure 2-3 where a wellbore is drilled vertically, the vertical stress represents the maximum principal stress which is also the same as the overburden stress. The horizontal stresses also represent the minimum and intermediate principal stresses (Aadnøy and Looyeh, 2011).

The principal stresses for a set of homogenous linear equations are given by the following equations:

$$[\sigma] = \begin{bmatrix} \sigma_x & \tau_{xy} & \tau_{xz} \\ \tau_{xy} & \sigma_y & \tau_{yz} \\ \tau_{xz} & \tau_{yz} & \sigma_z \end{bmatrix} = \begin{bmatrix} \sigma_1 & 0 & 0 \\ 0 & \sigma_2 & 0 \\ 0 & 0 & \sigma_3 \end{bmatrix} \quad 2.12$$

To solve for the principal stresses, the right-hand side is subtracted from the left-hand side and the determinant is taken:

$$\begin{vmatrix} \sigma_x - \sigma & \tau_{xy} & \tau_{xz} \\ \tau_{xy} & \sigma_y - \sigma & \tau_{yz} \\ \tau_{xz} & \tau_{yz} & \sigma_z - \sigma \end{vmatrix} = 0 \quad 2.13$$

Solving and simplifying the determinant results in a cubic equation below:

$$\sigma^3 - I_1\sigma^2 - I_2\sigma - I_3 = 0 \quad 2.14$$

where:

$$\begin{aligned} I_1 &= \sigma_x + \sigma_y + \sigma_z \\ I_2 &= \tau_{xy}^2 + \tau_{xz}^2 + \tau_{yz}^2 - \sigma_x\sigma_y - \sigma_x\sigma_z - \sigma_y\sigma_z \\ I_3 &= \sigma_x(\sigma_y\sigma_z - \tau_{yz}^2) - \tau_{xy}(\tau_{xy}\sigma_z - \tau_{xz}\tau_{yz}) + \tau_{xz}(\tau_{xy}\tau_{yz} - \tau_{xz}\sigma_y) \end{aligned} \quad 2.15$$

The invariants, I_1 , I_2 and I_3 do not change irrespective of the coordinate system orientation.

The solution of the cubic equation 2.14 would yield three real roots known as the principal stresses, σ_1 , σ_2 and σ_3 . σ_1 has the highest value while σ_3 has the least value (Aadnøy and Looyeh, 2011).

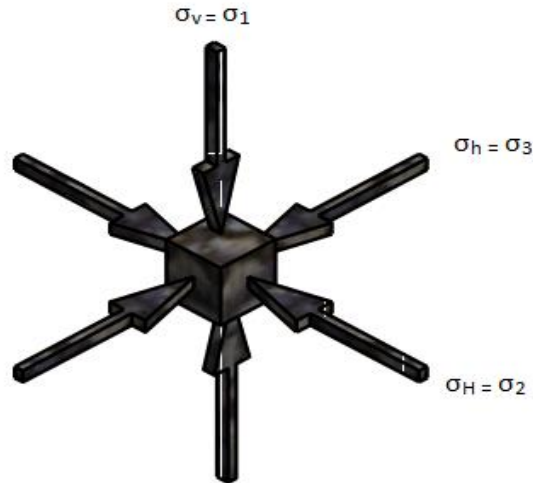


Figure 2-3 Principal In-situ stresses in a vertical borehole

2.11 Methods to Measure Stress

The different methods to measure the magnitude and direction of the horizontal in-situ stresses are generally categorized in three main groups. Below is a summary of the methods as presented by Carnegie et al. (2002):

1. Core Analysis
2. Logging technique
3. Formation Fracture technique

Core analysis involves retrieving core samples from well and performing different strain experiments like Anelastic Strain Recovery and Differential Strain Curve Analysis on the cores. The results obtained are interpreted and used to predict the direction and magnitude of the in-situ stresses. The challenge with this technique is some of the unverifiable assumptions made. Therefore, it is recommended to compare the results obtained here with results of other techniques with more credibility.

Logging technique is based on the interpretation of stress through a mechanistic model that makes use of borehole breakout measurement or some relationships that exist at or close to the face of the wellbore. The relationship is between the stresses and rock properties and it is semi-empirical. To determine the stresses, the Poisson's ratio obtained from sonic velocities is utilized. The stress vs depth profile is easily generated but in order to determine the absolute stress values, data from more accurate method like the micro fracturing technique are used for calibration.

Formation Fracture technique is a down hole fracturing method. The formation is pressurized until it fractures and measurements taken at different stages are used to compute or directly estimate the stresses. Tests such as Leak-off test, Extended leak-off test and Micro-Fracturing are some very popular examples. This thesis makes use of data obtained from this technique. More details of these tests would be given in later chapters.

2.12 Formation pore pressure

The rock matrix contains pores within which is filled with fluids. The fluids contained within the rock pores apply pressure on the surrounding walls due to the effect of overburden stress; this pressure is known as the formation pore pressure. The formation pore pressure varies according to geological effects in the area. Formation pore pressures are usually classified to be Normal, Abnormal or Subnormal. The normal formation pressure is 0.465psi/ft. which is the pore pressure of a formation with salt water as pore fluid. The pore pressure gradient of sea water is 0.43psi/ft. Pore pressure gradient higher than 0.465psi/ft. is referred to as abnormal pressure. This may be due to geological effects such as fault, salt dome intrusion or low permeability, which prevents the pore fluid from interacting with other fluids in the area hence, the fluid, is unable to transmit pressure and causing it to bear extra weight exerted by the overburden. The abnormal pore pressure can be as high as 0.8psi/ft. to 1psi/ft. Formation pore pressure is said to be subnormal when the pore pressure gradient is less than that of sea water (0.465psi/ft.). This may either be as a result of erosion of the overlaying formation in a region that experienced uplift or warping of lower and upper beds leaving the middle bed to spread to fill the space created by the warping and thereby experiencing a less pore pressure (Louden, 1972).

Over the years there have been technological advancements in the quest to accurately predict the formation pore pressure; there is no one generally accepted technology to accurately estimate the upper section of the formation (Peuchen and Klein, 2011). Comparing the various technologies, Peuchen and Klein (2011) added grading as shown in Table 2-2. The focus of this thesis is not on the determination of the formation pore pressure and hence, would not be discussed in more details.

Table 2-2: Technology for the prediction of tophole formation pore pressures. (Peuchen and Klein, 2011)

Technology	Mode	Applicability				Notes 1 and 2	Notes
		(A)	(B)	(C)	(D)		
Spatial Characterisation							
2-D/3-D geophysics, seismic reflection, electromagnetics	RS	--	--	+	++	Note 3. Dutta (2002), Bridges (2003), Young & Lepley (2005), Gutierrez et al. (2006)	
Profiling							
Logging While Drilling LWD and Pressure While Drilling PWD	IB	--	+/-	+/-	++	Natural gamma, neutron, electrical resistivity, resistivity and pressure at bit. Ostermeier et al. (2000), Bruce et al. (2003), Citta et al. (2003), Flemings et al. (2006)	
Geophysical downhole logging	BD, FS & IB	--	+/-	+	++	Calliper, natural gamma, neutron, seismic velocity, electrical resistivity. Nigbor and Imai (1994), Digby (2002), Hamilton et al. (2004)	
Non-pressure (core) sampling	BD & FS	--	--	++	++	Various systems available to suit sample quality and ground conditions. Kolk & Wegerif (2005)	
Cone Penetration Testing CPT	BD & FS	--	+/-	++	++	Common for geotechnical investigation. Peuchen (2000)	
Point Measurement							
Pore pressure dissipation testing PPDT with piezoprobe or piezocone penetrometer	BD & FS	++	++	++	+	Note 4. Davis et al. (1991), Ostermeier et al. (2000), Whittle et al. (2001), Dugan (2003), Orange et al. 2003, Flemings et al. (2006)	
Pressure (core) sampling	BD	+	+/-	++	+/-	Interference with drilling mud pressures cannot be fully prevented. Peuchen & Raap (2007)	
In-situ pore water sampling	BD	+/-	+/-	--	+	Suits shallow section, CPT-based deployment. Tervoort & Peuchen (2007)	
Packer testing: Leak Off Testing LOT, Formation Integrity Testing FIT, Hydraulic Fracture Testing HFT	IB	+	+	--	+/-	Applies resettable packer(s) Fierloos (2005)	
Wireline Formation Testing WFT	IB	--	+/-	--	+	Various systems, mostly targeting reservoir permeability. Eishahawi et al. (2008), Manin et al. (2005)	
Point Monitoring							
In-situ piezometer monitoring	BD & FS	++	++	+	+/-	Note 4. Usually requires site re-visit for data collection. Tjelta & Strout (2010), Strout & Tjelta (2005)	
Legend: (A) Formation pore pressure – fine grained formations (clay/shale) ++ high applicability (B) Formation pore pressure – coarse grained formations (sand) + medium applicability (C) Ground truthing for geotechnical/geological formation characteristics +/- low (possible) applicability (D) Deployment time/robustness -- no applicability BD intrusive, from Below Drillbit FS intrusive, directly From Seafloor IB In Borehole RS Remote Sensing							

2.13 Effective stress

The effective stress is a fraction of the total stress that the rock matrix bears. Since, the overburden stress is distributed between the rock grains and the fluid in the pores, the difference between the total stress, that is, the overburden and the pore pressure, which is the pressure taken up by the fluid is the effective stress of the rock formation. The importance of the knowledge of the effective stress is due to the significant effects it has on rock failure. Failure criteria applied to rocks will be based on the effective stress and not the total stress (Aadnøy and Looyeh, 2011).

The effective stress can be used to illustrate the stress state at any point in the subsurface. This is a principle developed by Terzaghi and hence, the equation:

$$\sigma_e = \sigma - P_o \quad 2.16$$

where σ_e is the effective stress, σ is the total stress and P_o is the pore pressure.

Based on reversible strain and linear elasticity, Biot introduced the concept of Effective stress coefficient (Alam et al., 2012), and added a constant which is referred to as Biot's constant and it's given by:

$$\sigma_e = \sigma - \beta P_o \quad 2.17$$

and

$$\beta = 1 - \frac{\text{Porous Matter}}{\text{Interpore Material}} = 1 - \frac{E}{E_i} \frac{1 - 2\nu_i}{1 - 2\nu} \quad 2.18$$

The Biot's, constant is calculated as shown in equation 2.18 and it is an estimation with a value for real rocks ranging from 0.8 to 1.0 (Aadnøy and Looyeh, 2011). The value of Biot's coefficient is a function of the pore fluid pressure exerted on the grain contact area. The stress differential ($\sigma - P_o$) changes with change in the pore pressure or the overburden stress. Strains in the rock occur as a result of an increase in the stress differential while decrease in the stress differential makes the rock to relax. The changes in the differential stress affect rock grains contact area and hence, the value of β (Alam et al., 2012). The changes in the effective stresses are solely responsible for effects like distortion, compression and shear resistance changes. This means that the rock strength, deformation and the change in volume are controlled by effective stress (Reyes and Osisanya, 2002).

2.14 State of stress

The stress state in the subsurface can either be Isotropic or Anisotropic. Isotropic, also known as hydrostatic stress field can be seen in an environment where the disposition is relaxed, all tectonic effects are neglected with the assumption that only the compaction of the overlying rock formation contribute to the horizontal in-situ stresses. In this case, it is logical to assume that the horizontal stresses are the same in all directions. Since the stresses are equal in all directions, the same value for leak-off is anticipated in cases of deviated boreholes. The overburden stress in this environment is higher than the horizontal stresses and as the borehole angle increases, the

fracture gradient decreases. This simple stress scenario is an ideal case and it is not common, in the real scenario stress states are convoluted.

The anisotropic stress state represents the real scenario found in most oil fields. In this stress state, the effects of topography, faults, plate tectonics or salt domes cause the horizontal stresses to vary with direction (Aadnoy and Looyeh, 2011).

2.15 Effect of Faulting on in-situ stresses

In a basin that is relaxed tectonically, it is expected that the overburden stress is the largest in magnitude while the minimum and maximum horizontal stresses are equal. However, the presence of faulting affects the magnitude of the in-situ stresses. Stresses found in a region that is experiencing Normal faulting, Reverse faulting and Strike-Slip faulting are categorized below,(Aadnoy and Hansen, 2005)

Normal fault stress state: $\sigma_v > \sigma_H > \sigma_h$

Reverse fault stress state: $\sigma_H > \sigma_h > \sigma_v$

Strike-slip fault stress state: $\sigma_H > \sigma_v > \sigma_h$

FJÆR et al. (2008) illustrated the faulting scenarios as shown in Figure 2-4, given that the directions of one of the principal stresses is vertical. When the largest of the principal stresses, σ_1 is vertical and the dip is greater than 45° , commonly about 60° , Normal fault occurs. Thrust fault is formed when the least principal stress, σ_3 is vertical, the hanging wall moves upward and the dip is smaller than 45° , usually about 30° . Strike-slip fault is formed when the intermediate principal stress, σ_2 is vertical and failure planes are formed which are vertical.

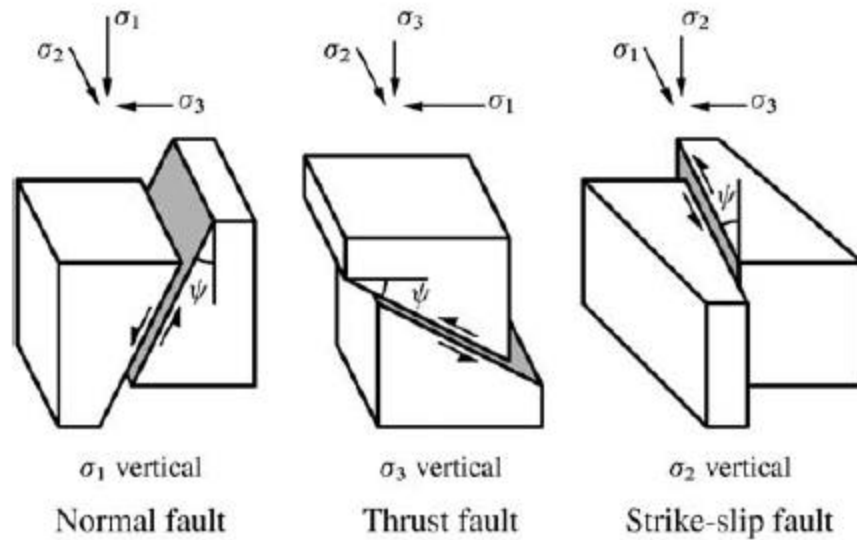


Figure 2-4: Fault types and associated stresses. (FJÆR et al., 2008)

2.16 In-situ stresses Bounds

The magnitude of the horizontal in-situ stresses determined should be verified to ensure that they are realistic values. In a borehole, irrespective of the wellbore angle, the collapse pressure can never at any point or instance be equal to the fracture pressure. A situation where, the values obtained for the horizontal stresses results in the two meeting is a clear indication of wrong estimation, see Figure 2-5. In any instance, the critical collapse pressure must always be lower than the critical fracture pressure (Aadnoy et al., 2013).

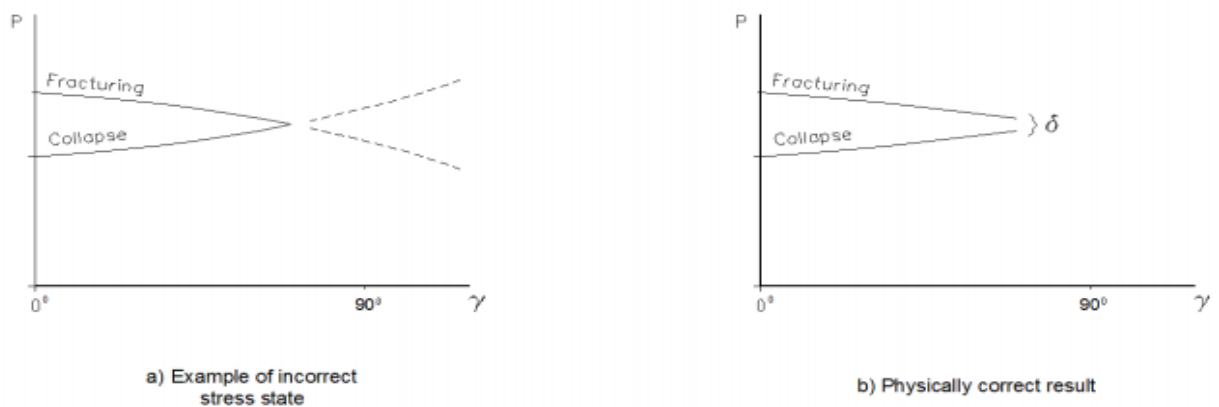


Figure 2-5: Plots of Collapse and Fracture pressure against wellbore inclination (Aadnoy et al., 2013)

After some analysis, the bounds on the in-situ are generalized by Aadnoy and Hansen (2005) and tabulated as shown in Table 3.

Table 3: In-situ stresses general bounds for Normal, Strike-slip and Reverse Faults.

Stress State	Upper Bound	Lower Bound
Normal Fault	$\frac{\sigma_H}{\sigma_v}, \frac{\sigma_h}{\sigma_v} \leq 1$	$\frac{\sigma_H}{\sigma_v}, \frac{\sigma_h}{\sigma_v} \geq \frac{B+C}{A}$
Strike/Slip Fault	$\frac{\sigma_H}{\sigma_v} \leq \frac{A-C}{B}, \quad \frac{\sigma_h}{\sigma_v} \leq 1$	$\frac{\sigma_H}{\sigma_v} \geq 1, \quad \frac{\sigma_h}{\sigma_v} \geq \frac{B+C}{A}$
Reverse Fault	$\frac{\sigma_H}{\sigma_v}, \frac{\sigma_h}{\sigma_v} \leq \frac{A-C}{B}$	$\frac{\sigma_H}{\sigma_v}, \frac{\sigma_h}{\sigma_v} \geq 1$

where: $A = 7 - \sin\phi$, $B = 5 - 3\sin\phi$, $C = \frac{2P_o(1+\sin\phi)+2(\delta-\tau_o\cos\phi)}{\sigma_v}$

2.17 Distribution of Stresses around a wellbore

The above section presented the ideal scenario of the magnitude and orientation of the in-situ stresses, unfortunately, the real life situation is far from ideal. The layers of the rock formation are not usually nicely arranged horizontally and perfectly. In addition to that, drilling of a circular hole creates a void and thereby affects the stresses. This section takes a look at the stresses that are present at the walls and surroundings of the drilled hole.

The stresses in an undisturbed formation are usually compressive. The three principal in-situ stresses are said to be in equilibrium and stable before any digging is done and if there is no seismic operation close by. Immediately a hole is drilled in the formation, the original distribution of the stresses is altered and this creates a reorganization of the stresses around the drilled hole (Aadnøy and Looyeh, 2011). The drilled hole is kept open by the drilling mud. The drilling mud also reacts with the formation and contributes to instability problems in the formation. The pressure exerted by the drilling mud on the formation cannot be an exact replacement of the in-situ stresses of the original undisturbed formation, thus, altering the in-situ stresses. FJÆR et al. (2008) pointed out that the resultant deviatoric stresses may exceed the

formation capacity and lead to failure of the rock formation. Figure 2-6 illustrates an example of the stresses in a drilled borehole.

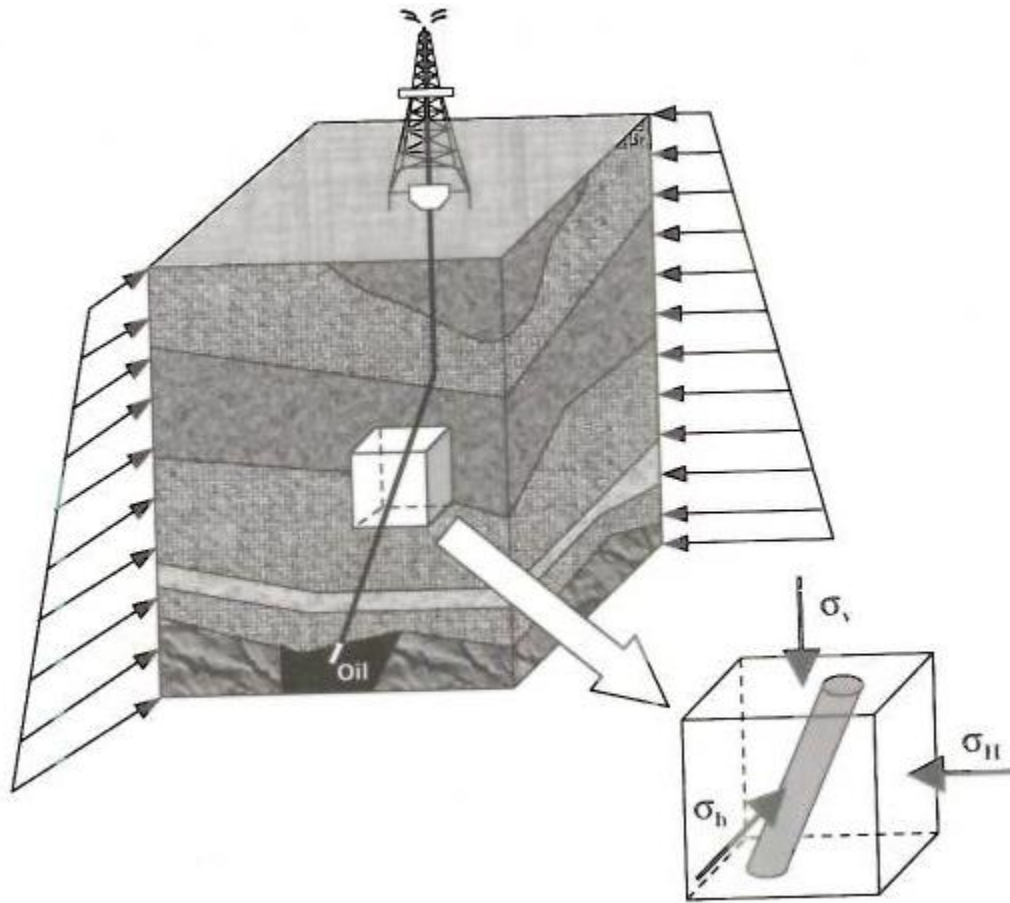


Figure 2-6: A schematic showing in-situ stresses around a wellbore (Aadnøy and Looyeh, 2011).

In order to investigate the state of the stresses in the Figure 2-6, Aadnøy and Looyeh (2011) transformed the in-situ stresses to illustrate a formation with uniform stress state before the hole is drilled and another to show the stress concentration formed and change in stress state as a result of change in geometry due to the circular hole drilled. These are shown in Figure 2-7

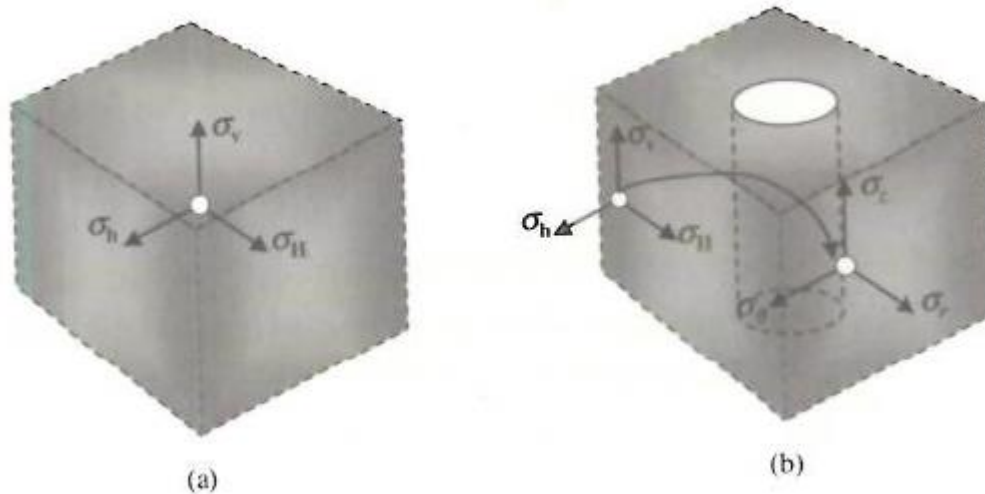


Figure 2-7: (a) Rock formation with uniform stress state, (b) Rock formation with a drilled hole where the stress state will change. (Aadnøy and Looyeh, 2011)

Aadnøy and Looyeh (2011) explained that while drilling into a rock formation, we may encounter two different set of stresses namely:

1. The in-situ stresses which are also called far-field stresses.
2. The stresses around the wellbore.

2.18 Stress analysis equations

Aadnøy and Looyeh (2011) also classified the real rock structure as a statically indeterminate system. To resolve the stress state, it is required to satisfy and solve three simultaneous equations. The equations are:

1. Equations of equilibrium
2. Equations of compatibility
3. Constitutive relations.

The model presented is based on the Kirsch, 1898.

2.18.1 Equations of equilibrium

A Cartesian coordinate system is used to represent the stress state shown in Figure 2-7(b). Assuming the plate is extensive and the stresses are in a state of equilibrium. The following ensues:

$$\begin{aligned}
 \frac{\partial \sigma_x}{\partial x} + \frac{\partial \tau_{xy}}{\partial y} + \frac{\partial \tau_{xz}}{\partial z} + F_x &= 0 \\
 \frac{\partial \tau_{xy}}{\partial x} + \frac{\partial \sigma_y}{\partial y} + \frac{\partial \tau_{yz}}{\partial z} + F_y &= 0 \\
 \frac{\partial \tau_{xz}}{\partial x} + \frac{\partial \tau_{yz}}{\partial y} + \frac{\partial \sigma_z}{\partial z} + F_z &= 0
 \end{aligned}
 \tag{2.19}$$

The stress state represents the normal (σ) and shear (τ) stress components and body forces (F) applied in the directions of x , y and z . Representing equations 2.19 in the cylindrical coordinate system:

$$\begin{aligned}
 \frac{\partial \sigma_r}{\partial r} + \frac{1}{r} \frac{\partial \tau_{r\theta}}{\partial \theta} + \frac{\partial \tau_{rz}}{\partial z} + \frac{\sigma_r - \sigma_\theta}{r} + F_r &= 0 \\
 \frac{\partial \tau_{r\theta}}{\partial r} + \frac{1}{r} \frac{\partial \sigma_\theta}{\partial \theta} + \frac{\partial \tau_{\theta z}}{\partial z} + \frac{2\tau_{r\theta}}{r} + F_\theta &= 0 \\
 \frac{\partial \tau_{rz}}{\partial r} + \frac{1}{r} \frac{\partial \tau_{\theta z}}{\partial \theta} + \frac{\partial \sigma_z}{\partial z} + \frac{\tau_{rz}}{r} + F_z &= 0
 \end{aligned}
 \tag{2.20}$$

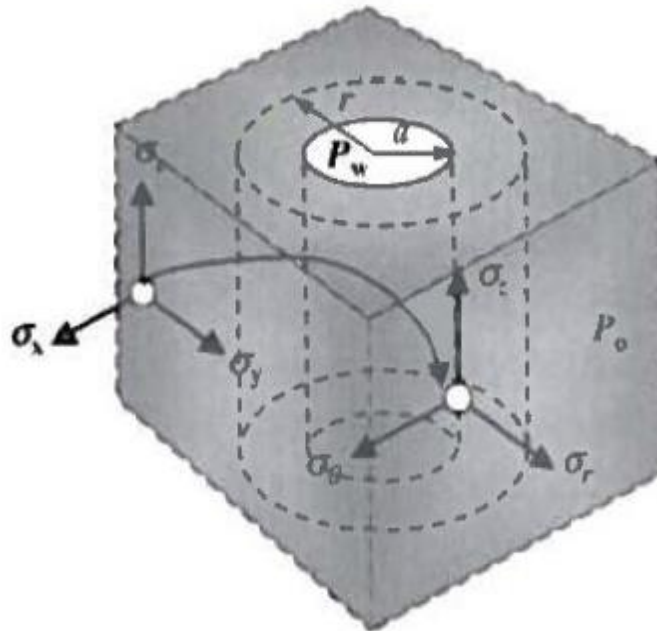


Figure 2-8: Stresses position around a borehole. (Aadnøy and Looyeh, 2011)

With the assumption that the borehole is symmetrical about its axis boundary loads will act along and perpendicular to the axis:

$$\tau_{rz} = \tau_{\theta z} = \gamma_{rz} = \gamma_{\theta z} = 0 \quad 2.21$$

Equation 2.12 can further be simplified to yield:

$$\begin{aligned} \frac{\partial \sigma_r}{\partial r} + \frac{1}{r} \frac{\partial \tau_{r\theta}}{\partial \theta} + \frac{\sigma_r - \sigma_\theta}{r} + F_r &= 0 \\ \frac{\partial \tau_{r\theta}}{\partial r} + \frac{1}{r} \frac{\partial \sigma_\theta}{\partial \theta} + \frac{2\tau_{r\theta}}{r} + F_\theta &= 0 \\ \frac{\partial \sigma_z}{\partial z} + F_z &= 0 \end{aligned} \quad 2.22$$

Because of rotational symmetry, Equation 2.22 will be reduced to:

$$\begin{aligned} \frac{\partial \sigma_r}{\partial r} + \frac{\sigma_r - \sigma_\theta}{r} + F_r &= 0 \\ \frac{\partial \sigma_z}{\partial z} + F_z &= 0 \end{aligned} \quad 2.23$$

2.18.2 Compatibility equations

These equations satisfy the condition that the stresses and strains must be compatible as the rock formation experience deformation when loaded. The equations are six but only one is shown below:

$$\frac{\partial^2 \varepsilon_x}{\partial y^2} + \frac{\partial^2 \varepsilon_y}{\partial x^2} = \frac{\partial^2 \gamma_{xy}}{\partial x \partial y} \quad 2.24$$

and in cylindrical coordinate system:

$$\frac{\partial^2 \varepsilon_r}{\partial \theta^2} + \frac{\partial^2 \varepsilon_\theta}{\partial r^2} = \frac{\partial^2 \gamma_{r\theta}}{\partial r \partial \theta} \quad 2.25$$

where:

$$\begin{aligned}
 [\varepsilon] &= \begin{bmatrix} \varepsilon_r & \frac{1}{2}\gamma_{r\theta} & \frac{1}{2}\gamma_{rz} \\ \frac{1}{2}\gamma_{r\theta} & \varepsilon_\theta & \frac{1}{2}\gamma_{\theta z} \\ \frac{1}{2}\gamma_{rz} & \frac{1}{2}\gamma_{\theta z} & \varepsilon_z \end{bmatrix} \\
 &= \begin{bmatrix} \frac{\partial u}{\partial r} & \frac{1}{2}\left(\frac{1}{r}\frac{\partial u}{\partial \theta} + \frac{\partial v}{\partial r} - \frac{v}{r}\right) & \frac{1}{2}\left(\frac{\partial w}{\partial r} + \frac{\partial u}{\partial z}\right) \\ \frac{1}{2}\left(\frac{1}{r}\frac{\partial u}{\partial \theta} + \frac{\partial v}{\partial r} - \frac{v}{r}\right) & \frac{1}{r}\frac{\partial v}{\partial \theta} + \frac{u}{r} & \frac{1}{2}\left(\frac{\partial v}{\partial z} + \frac{1}{r}\frac{\partial w}{\partial \theta}\right) \\ \frac{1}{2}\left(\frac{\partial w}{\partial r} + \frac{\partial u}{\partial z}\right) & \frac{1}{2}\left(\frac{\partial v}{\partial z} + \frac{1}{r}\frac{\partial w}{\partial \theta}\right) & \frac{\partial w}{\partial z} \end{bmatrix}
 \end{aligned} \tag{2.26}$$

u , v and w represents body displacements in the coordinate system directions, r , θ and z .

2.18.3 Constitutive relations

Hooke's law is used here as the governing equation to relate the stresses and strains developed in the rock formation. A presentation of the equations in Cartesian and cylindrical coordinate systems is given with the inference that the rock material is isotropic:

$$\begin{bmatrix} \sigma_x \\ \sigma_y \\ \sigma_z \end{bmatrix} = \frac{E}{(1+\nu)(1-2\nu)} \begin{bmatrix} 1-\nu & \nu & \nu \\ \nu & 1-\nu & \nu \\ \nu & \nu & 1-\nu \end{bmatrix} \begin{bmatrix} \varepsilon_x \\ \varepsilon_y \\ \varepsilon_z \end{bmatrix} \tag{2.27}$$

$$\begin{bmatrix} \tau_{xy} \\ \tau_{yz} \\ \tau_{xz} \end{bmatrix} = G \begin{bmatrix} \gamma_{xy} \\ \gamma_{yz} \\ \gamma_{xz} \end{bmatrix} \tag{2.28}$$

in cylindrical coordinate system:

$$\begin{bmatrix} \sigma_r \\ \sigma_\theta \\ \sigma_z \end{bmatrix} = \frac{E}{(1+\nu)(1-2\nu)} \begin{bmatrix} 1-\nu & \nu & \nu \\ \nu & 1-\nu & \nu \\ \nu & \nu & 1-\nu \end{bmatrix} \begin{bmatrix} \varepsilon_r \\ \varepsilon_\theta \\ \varepsilon_z \end{bmatrix} \tag{2.29}$$

$$\begin{bmatrix} \tau_{r\theta} \\ \tau_{\theta z} \\ \tau_{rz} \end{bmatrix} = G \begin{bmatrix} \gamma_{r\theta} \\ \gamma_{\theta z} \\ \gamma_{rz} \end{bmatrix} \tag{2.30}$$

expressing strains as a function of stresses:

$$\begin{bmatrix} \varepsilon_x \\ \varepsilon_y \\ \varepsilon_z \end{bmatrix} = \frac{1}{E} \begin{bmatrix} 1 & -\nu & -\nu \\ -\nu & 1 & -\nu \\ -\nu & -\nu & 1 \end{bmatrix} \begin{bmatrix} \sigma_x \\ \sigma_y \\ \sigma_z \end{bmatrix} \quad 2.31$$

$$\begin{bmatrix} \gamma_{xy} \\ \gamma_{yz} \\ \gamma_{xz} \end{bmatrix} = \frac{1}{G} \begin{bmatrix} \tau_{xy} \\ \tau_{yz} \\ \tau_{xz} \end{bmatrix} \quad 2.32$$

$$\begin{bmatrix} \varepsilon_r \\ \varepsilon_\theta \\ \varepsilon_z \end{bmatrix} = \frac{1}{E} \begin{bmatrix} 1 & -\nu & -\nu \\ -\nu & 1 & -\nu \\ -\nu & -\nu & 1 \end{bmatrix} \begin{bmatrix} \sigma_r \\ \sigma_\theta \\ \sigma_z \end{bmatrix} \quad 2.33$$

$$\begin{bmatrix} \gamma_{r\theta} \\ \gamma_{\theta z} \\ \gamma_{rz} \end{bmatrix} = \frac{1}{G} \begin{bmatrix} \tau_{r\theta} \\ \tau_{\theta z} \\ \tau_{rz} \end{bmatrix} \quad 2.34$$

2.18.4 Boundary condition

For a Cartesian coordinate system, equations 2.19, 2.24, 2.31 and 2.32 are used or equations 2.20, 2.25, 2.33 and 2.34 for a cylindrical coordinate system. These simultaneous equations are solved by applying boundary conditions. The conditions at the boundaries are:

$$\begin{aligned} \sigma_r &= P_w, & \text{at } r &= a \\ \sigma_r &= \sigma_a, & \text{at } r &= \infty \end{aligned} \quad 2.35$$

where a = wellbore radius.

In order to get the stresses at the wall of the borehole, Aadnøy and Looyeh (2011) itemized the following steps to be taken in the order presented:

1. Identify the principal in-situ stress state ($\sigma_v, \sigma_H, \sigma_h$)
2. Transform the identified principal stress state to the stress state ($\sigma_x, \sigma_y, \sigma_z$), defined with respect to the Cartesian coordinate system attached to the wellbore.

3. Use the sets of equations defined in section 2.18 and find the stress state $(\sigma_r, \sigma_\theta, \sigma_z)$, with respect to the cylindrical coordinate system attached to the wellbore, in terms of the stress state $(\sigma_x, \sigma_y, \sigma_z)$.
4. Find the stress state at the wellbore wall $(\sigma_r, \sigma_\theta, \sigma_z)_{r=a}$ by replacing r with a , the radius of the wellbore.

2.18.5 Stress transformation and equations

The principal in-situ stresses in the rock formation need to be transformed to a different Cartesian coordinate system to align with the orientation of the drilled hole. The stress and direction of the drilled wellbore is defined by its inclination, γ , which is the angle with respect to the vertical, the Azimuth, φ and the position of the wellbore with reference to the x-axis, θ , (Aadnøy and Looyeh, 2011).

The transformation of the stress components yields the subsequent equations:

$$\begin{aligned}
 \sigma_x &= (\sigma_H \cos^2 \varphi + \sigma_h \sin^2 \varphi) \cos^2 \gamma + \sigma_v \sin^2 \gamma \\
 \sigma_y &= \sigma_H \sin^2 \varphi + \sigma_h \cos^2 \varphi \\
 \sigma_{zz} &= (\sigma_H \cos^2 \varphi + \sigma_h \sin^2 \varphi) \sin^2 \gamma + \sigma_v \cos^2 \gamma \\
 \tau_{xy} &= \frac{1}{2} (\sigma_h - \sigma_H) \sin 2\varphi \cos \gamma \\
 \tau_{xz} &= \frac{1}{2} (\sigma_H \cos^2 \varphi + \sigma_h \sin^2 \varphi - \sigma_v) \sin 2\gamma \\
 \tau_{yz} &= \frac{1}{2} (\sigma_h - \sigma_H) \sin 2\varphi \sin \gamma
 \end{aligned} \tag{2.36}$$

After the successful transformation of the stress equations as given by equation 2.36, steps 1 and 2 are completed. In order to achieve steps 3 and 4, governing equations were developed, some logical assumptions made and boundary conditions applied, the resultant Kirsch Equations defined as follows:

$$\begin{aligned}
 \sigma_r &= \frac{1}{2}(\sigma_x + \sigma_y) \left(1 - \frac{a^2}{r^2}\right) + \frac{1}{2}(\sigma_x - \sigma_y) \left(1 + 3\frac{a^4}{r^4} - 4\frac{a^2}{r^2}\right) \cos 2\theta \\
 &\quad + \tau_{xy} \left(1 + 3\frac{a^4}{r^4} - 4\frac{a^2}{r^2}\right) \sin 2\theta + \frac{a^2}{r^2} P_w \\
 \sigma_\theta &= \frac{1}{2}(\sigma_x + \sigma_y) \left(1 + \frac{a^2}{r^2}\right) - \frac{1}{2}(\sigma_x - \sigma_y) \left(1 + 3\frac{a^4}{r^4}\right) \cos 2\theta \\
 &\quad - \tau_{xy} \left(1 + 3\frac{a^4}{r^4}\right) \sin 2\theta - P_w \frac{a^2}{r^2} \\
 \sigma_z &= \sigma_{zz} - 2\nu(\sigma_x - \sigma_y) \frac{a^2}{r^2} \cos 2\theta - 4\nu\tau_{xy} \frac{a^2}{r^2} \sin 2\theta \rightarrow \text{Plane Strain} \\
 \sigma_z &= \sigma_{zz} \rightarrow \text{Plane Stress} \\
 \tau_{r\theta} &= \left[\frac{1}{2}(\sigma_x - \sigma_y) \sin 2\theta + \tau_{xy} \cos 2\theta \right] \left(1 - 3\frac{a^4}{r^4} + 2\frac{a^2}{r^2}\right) \\
 \tau_{rz} &= (\tau_{xy} \cos \theta + \tau_{yz} \sin \theta) \left(1 - \frac{a^2}{r^2}\right) \\
 \tau_{\theta z} &= (-\tau_{xz} \sin \theta + \tau_{yz} \cos \theta) \left(1 + \frac{a^2}{r^2}\right)
 \end{aligned} \tag{2.37}$$

Considering an isotropic solution, and taking $r = a$, equation 2.37 becomes:

$$\begin{aligned}
 \sigma_r &= P_w \\
 \sigma_\theta &= \sigma_x + \sigma_y - P_w - 2(\sigma_x - \sigma_y) \cos 2\theta - 4\tau_{xy} \sin 2\theta \\
 \sigma_z &= \sigma_{zz} - 2\nu(\sigma_x - \sigma_y) \cos 2\theta - 4\nu\tau_{xy} \sin 2\theta \rightarrow \text{Plane Strain} \\
 \sigma_z &= \sigma_{zz} \rightarrow \text{Plane Stress} \\
 \tau_{r\theta} &= 0 \\
 \tau_{rz} &= 0 \\
 \tau_{\theta z} &= 2(-\tau_{xz} \sin \theta + \tau_{yz} \cos \theta)
 \end{aligned} \tag{2.38}$$

3.0 Failure Models and Criteria

As mentioned in the previous section, in order to determine the in-situ stresses, data obtained from the failure of the rock formation are utilized in various models developed by researchers. This section looks at some failure criteria and some of the models widely used in the petroleum industry.

3.1 Failure Criteria

All failures must be based on some criterion. Different materials fail differently. For example, sands may fail in shear while clay failure may be as a result of plastic deformation. For every individual problem, appropriate failure criteria need to be carefully selected. Aadnøy and Looyeh (2011) highlighted some of the mechanisms which can affect the wellbore stability and eventually lead to rock formation failure as follows:

- Rock formation part due to Tensile failure
- Shear failure without appreciable plastic deformation
- Plastic deformation that may result to pore collapse
- Erosion or cohesive failure
- Creep failure which may lead to a tight hole situation during drilling
- Pore collapse or complete failure which may occur during production

Failure envelopes are developed using the failure criteria. The failure envelopes distinguish the stable or safe regions from the unstable or failed regions.

Some of the failure criteria commonly used in the oil and gas industry in analyzing rock failure during drilling is presented briefly;

3.1.1 The Von Mises Failure Model

Developed by Von Mises in the early twentieth century and has gained reputation over the years. Its application cuts across various engineering materials. The criterion makes use of the effective average stress and the second deviatoric invariant. In a tri-axial test, with the assumption that $\sigma_1 > \sigma_2 = \sigma_3$, the second deviatoric invariant is given as;

$$\sqrt{J_2} = \frac{1}{\sqrt{3}}(\sigma_1 - \sigma_3) \quad 3.1$$

based on the same assumption, the effective average stress as discussed in the previous chapter is defined as;

$$\sigma_m - P_o = \frac{1}{3}(\sigma_1 + 2\sigma_3) - P_o \quad 3.2$$

To create the failure envelope (Figure 3-1), the second deviatoric invariant is plotted on the y-axis against the effective average stress on the x-axis for varying axial loads σ_1 and confining pressures σ_3 . The plot shows two distinct regions, the safe and stable region below the curve and failed and unstable region above the curve (Aadnøy and Looyeh, 2011).

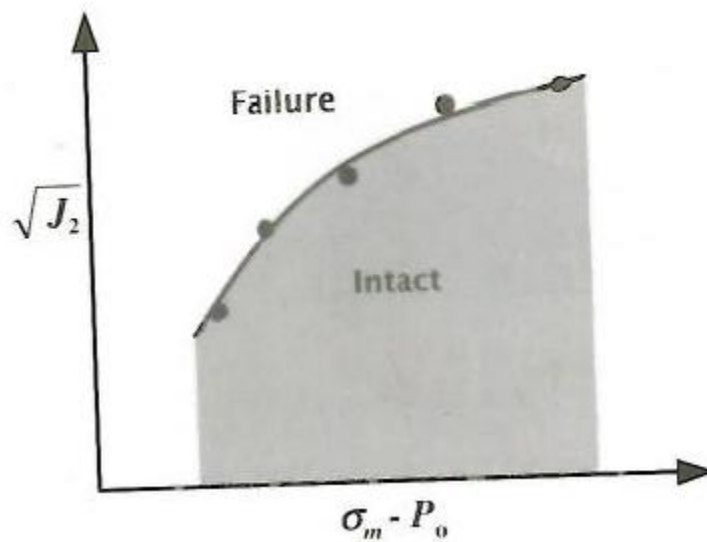


Figure 3-1 Von Mises failure envelope from triaxial test data (Aadnøy and Looyeh, 2011)

3.1.2 Mohr-Coulomb Failure Criterion

The Mohr-Coulomb criterion expresses a relationship between the shearing resistance, contact force and friction and as they relate to the bonds present in the rock grains. Mathematically, the criterion can be represented as:

$$\tau = \tau_0 + \sigma \tan \phi \quad 3.3$$

where τ is equal to the shear stress, τ_0 is the cohesive strength which is equivalent to the rock shear strength in the absence of any normal stress, σ is the effective normal stress which acts on the rock grains, ϕ is the internal friction angle which in drilling, is a surface's angle of inclination required to cause a superincumbent block to slide down the surface. They are coefficients and are determined from experiments. This criterion is exclusively based on shear failure and should be applied only to valid situations, trying to apply it to other failure mechanisms often result in an aberration from a straight line.

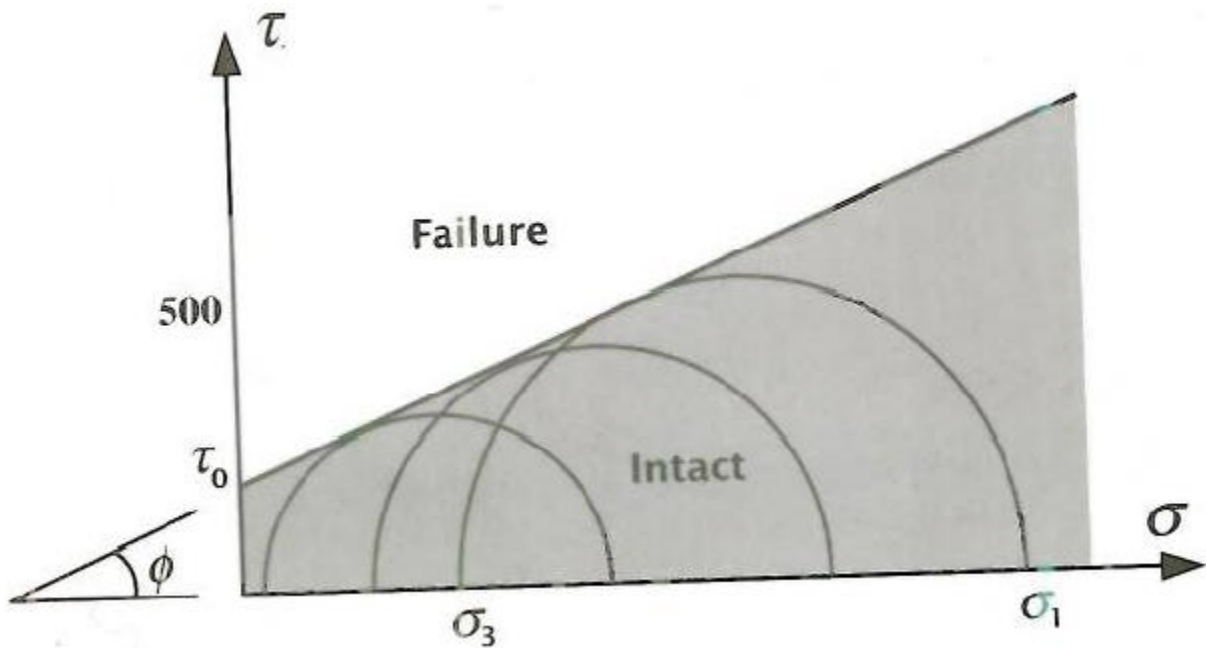


Figure 3-2 Mohr-Coulomb failure envelope from triaxial test data (Aadnøy and Looyeh, 2011)

The failure envelope as illustrated in Figure 3-2 is a composition of many Mohr's circles with each of the circles representing a triaxial test (Aadnøy and Looyeh, 2011).

3.1.3 The Griffith Failure Criterion

The Griffith failure criterion is 'applicable to materials which break in tension due to the presence of an existing microjack'. As the crack progresses, to attain the required surface energy enough energy must be released. The strain energy rate released must be greater than or at least equal to required increase in surface energy. The failure criterion is applicable to both cases of plane strain and plane stress in compression and tension. At the onset of a crack, the equation below is applicable for tensile failure:

$$\sigma_t = \sqrt{\frac{keE}{a}} \quad 3.4$$

where σ_t is the applied uniaxial tensile stress at failure, a as shown in Figure 3-3, is one half of initial crack length, E is the Young's modulus, e is the unit crack surface energy and k is a variable parameter depending on the testing conditions, for example, for plane stress, $k = 2/\pi$ and for plane strain, $k = 2(1 - \nu^2)/\pi$. Based on the criterion, a relationship between the triaxial compressive stress and the uniaxial tensile stress is derived (Aadnøy and Looyeh, 2011);

$$(\sigma_1 - \sigma_3)^2 = -8\sigma_t(\sigma_1 + \sigma_3) \quad 3.5$$

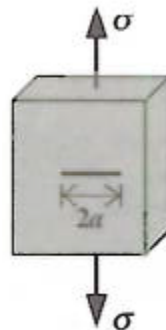


Figure 3-3 A test specimen Griffith criterion (Aadnøy and Looyeh, 2011)

3.1.4 Hoek-Brown Failure Criterion

Hoek and Brown in 1980 introduced this failure criterion which is completely empirical and usually applied to reservoirs with natural fractures. The criterion is developed based on data from triaxial test as shown in Figure 3-4. It is suitable in brittle failure but does not give a good result in brittle failure hence, its application for predicting failure is limited to formations with natural fracture. The criterion is presented as:

$$\sigma_1 = \sigma_3 + \sqrt{I_f \sigma_c \sigma_3 + I_i \sigma_c^2} \quad 3.6$$

I_f , I_i and σ_c are all measured parameters from the laboratory, where I_f is frictional index, I_i , the intact index and σ_c is crack stress parameter (Aadnøy and Looyeh, 2011).

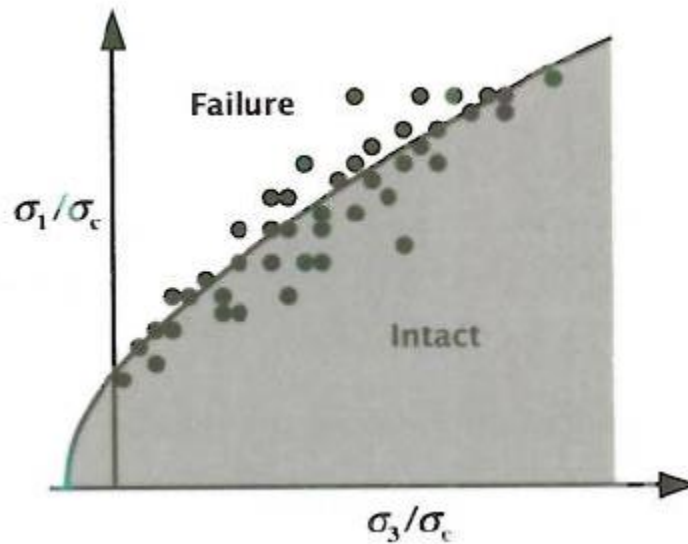


Figure 3-4 Hoek-Brown failure model using triaxial test data (Aadnøy and Looyeh, 2011)

3.1.5 The Drucker-Prager Failure Criterion

In this criterion, Drucker and Prager (1952) modified the Von Mises criterion with the assumption that the octahedral shear stress attains a critical value. Their modified equation is given as:

$$\alpha I_1 + \sqrt{J_2} - \beta = 0 \quad 3.7$$

α and β are material parameters and for a linear condition, are linked to the internal friction angle ϕ and cohesive strength, τ_o . A problem related to failure in rock formation can be evaluated at failure conditions by plotting the second deviatoric invariant $\sqrt{J_2}$, against the first invariant I_1 . It is suitable for high stress level (Aadnøy and Looyeh, 2011).

3.1.6 The Mogi-Coulomb Failure Criterion

Al-Ajmi and Zimmerman introduced this criterion after the conduction of a broad review of models of rock failure. The criterion is a modification of the Mohr-Coulomb criterion that resulted in a polyaxial state of stress where $\sigma_1 \neq \sigma_2 \neq \sigma_3$. Based on the results of test carried out using various models on different rock type failure data, they discovered that the Mohr-Coulomb criterion gives an underestimation of the strength of the rock while the Drucker-Prager criterion gives an overestimated result. Al-Ajmi and Zimmerman reveal that the Mogi-Coulomb failure criterion is the best fit by claiming that the intermediate principal stress has effects on failure. The equation summarized the criterion;

$$\tau_{oct} = k + m\sigma_{oct} \quad 3.8$$

where τ_{oct} is the octahedral shear stress and σ_{oct} is the octahedral normal stress and given as follow;

$$\tau_{oct} = \frac{1}{3} \sqrt{(\sigma_1 - \sigma_2)^2 + (\sigma_1 - \sigma_3)^2 + (\sigma_2 - \sigma_3)^2} = \sqrt{\frac{2}{3}} J_2 \quad 3.9$$

$$\sigma_{oct} = \frac{1}{3} (\sigma_1 + \sigma_2 + \sigma_3)$$

A plot of τ_{oct} against σ_{oct} as shown in Figure 3-5 gives a failure envelope, the material constants m and k can be determined form the slope and intercept of the graph.

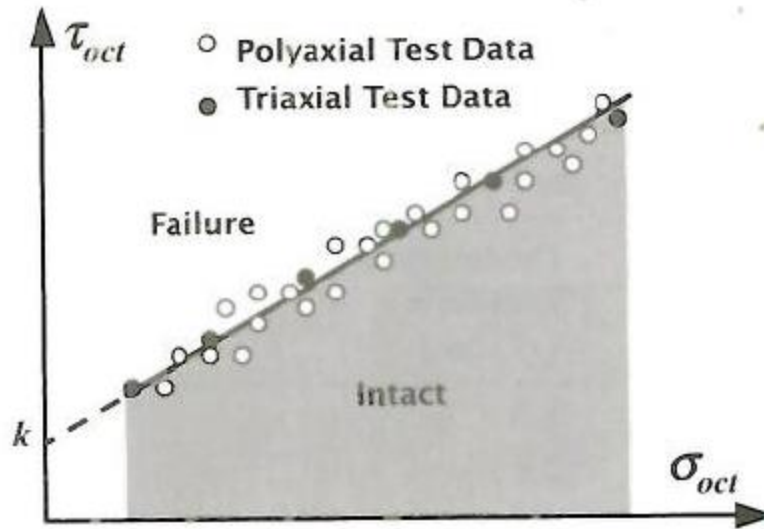


Figure 3-5 Mogi-Coulomb failure envelope for Triaxial and polyaxial data (Aadnøy and Looyeh, 2011)

For hard sedimentary rocks formations, according to Al-Ajmi and Zimmerman, this criterion is the most accurate failure model currently available (Aadnøy and Looyeh, 2011).

3.2 Mechanisms of Failure

Wellbore may fail due to various reasons. Generally, it is widely accepted that wellbore failure can be categorized into two primary groups (Aadnøy, 2010) :

1. Wellbore collapse.
2. Wellbore fracture.

3.3 Wellbore Collapse

Collapse of borehole is a shear failure and occurs when the pressure inside the hole is low. High circumferential stress, that is greater than the formation rock strength act around the wellbore. Shear failure result due to significant difference between the circumferential and radial stresses. Collapse can happen in the form of the rocks yielding or various failure models have been developed based on wellbore collapse. Much emphasis would not be placed here on the collapse models.

3.4 Wellbore Fracture

As opposed to wellbore collapse, wellbore fracture is a tensile failure and it is associated with high wellbore pressure. This failure mechanism is the most important when dealing with rocks because they are weak in tension. The circumferential stress reduces due to increase in the borehole pressure. The reduction in the circumferential stress leads to values lower than the formation rock tensile strength and hence, failure. According to Aadnoy and Chenevert (1987) ‘tensile failure occurs when the least effective principal stress exceeds the rock tensile strength’.

mathematically,

$$\sigma_{\theta} - P_o \leq \sigma_{tensile} \quad 3.10$$

3.5 Fracture gradient

The fracture gradient represents the slope profile of the fracture pressure in a rock formation. At any depth, the fracture pressure is the pressure required to initiate fractures in the formation. It is very important to be able to accurately estimate the fracture gradient of the formation in order to prevent lost circulation while drilling and it also has a direct influence on casing strings design. In drilling, the upper limit of the mud weight window is taken as the fracture gradient. The leak-off pressure (LOP) obtained from the leak-off test (LOT) is normally considered by the drilling engineers as the fracture gradient. Geomechanical engineers disagree and maintain that the fracture gradient should be the minimum horizontal stress. The upper limit of the mud weight is arbitrarily defined if there is no documentation of tensile failure at the wellbore. The upper limit of the mud weight window becomes contentious when wellbore tensile failure is noticed (Bai, 2011). Generally, fracture gradients can be determined by the following technique:

1. Experimentally or direct method.
2. Theoretically or indirect method.

3.5.1 Experimental or direct method

The experimental method which is a direct approach is obtained from tests from field by performing Pressure integrity tests; Leak-off test (Altun et al., 1999), Extended Leak-off test (Addis et al., 1998) or Micro-Fracturing (Carnegie et al., 2002). It involves the pumping of high

pressured fluid into the wellbore after the casing is set to induce fracture in the open formation below the casing shoe, which is assumed to be the weakest area. The technique is generally similar for all the tests mentioned, the difference is at the time the measurement is taken.

To get a summarized overview of the pressure integrity tests, it is important to begin with the **Formation integrity test (FIT)**. The formation integrity test is performed by pressurizing the well to a specific pressure to verify if the next open hole section is safe for further drilling. After the casing is cemented in place, the next open hole section is drilled to about 3 meters in order to carry out the FIT. The annulus is closed and mud is pumped into the well at rate of 40 to 50 liters per minute. As no circulation is allowed during the pumping, pressure builds up until the pre-determined pressure required to drill the next hole section is attained. From the Figure 3-6, the FIT test is stopped anywhere below the Leak off pressure (LOP), (Addis et al., 1998).

The leak-off test (LOT) is a form of the FIT but in this case, the pumping in the well is not stopped when a pre-set pressure is attained but the formation pressure is increased by the continuous pumping of mud until the formation is fractured. The fractured formation is noted when there is a decline in the rate of pressure increase in the well, signifying an increase in the system compressibility. As shown in Figure 3-6, the test is stopped after the LOP and measurements recorded.

For the **Extended leak-off test (XLOT)**, as the name implies, it is an extension of the Leak-off test. The pumping is not stopped after the initiation of fracture is observed but continues as fracture propagates and exceeds the fracture breakdown pressure, (FBP in Figure 3-6). After then, the pumps are stopped and the well monitored as the pressure declines and measurements are taken at the fracture closing pressure. The test is usually repeated for a minimum of two times.

In the **Micro-fracturing method**, which is referred to be the most accurate method to obtain fracture data, a small section of the open hole of about 3ft is isolated and tested with the aid of inflatable straddle packers. The open hole section normally would be imaged before the test to make sure that no fractures or weaknesses pre-exist. A down hole pump is used to pump the fluid used for the fracturing test. The pump and measuring gauges for fracture initiation pressure, fracture propagation pressure and fracture closure pressure are located down hole and in close

proximity to the section to be fractured. This minimizes the effect of compressibility on the pressure measurement. To ensure that the measured data are not impressed by stress concentrations in the vicinity of the wellbore, the method propagates the fracture at a distance of over four wellbore radii from the well (Carnegie et al., 2002) .

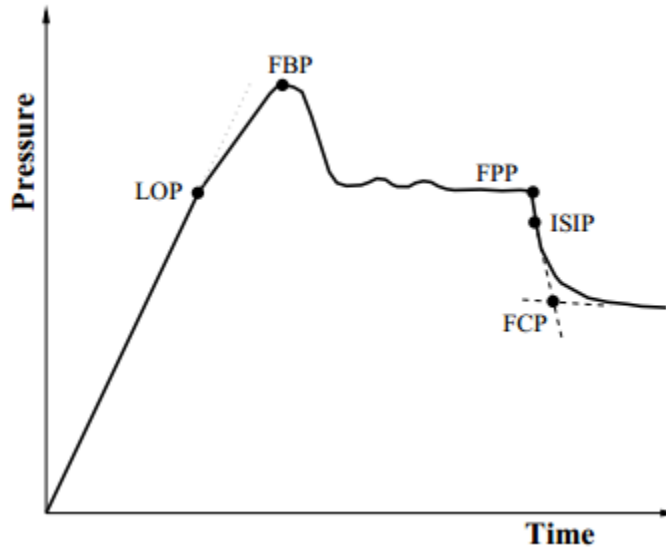


Figure 3-6: A plot showing the change in surface pressure during Extended Leak off test (Raaen et al., 2006)

To calculate the fracture pressure using data from wellbore fracture, Aadnoy and Chenevert (1987) gave the following equation:

$$P_{wf} = 3\sigma_y - \sigma_x - P_o + \sigma_{tensile} \quad 3.11$$

3.5.2 Theoretical or indirect method

For the theoretical method which is an indirect approach, various methods have been proposed by many authors (Hubbert and Willis (1957) , **Mathews and Kelly (1967)**, Pennebaker (1968), Eaton (1969), and Christman (1973)). All the methodologies by the all the authors take into account the effect of the pore pressure gradient. They all agree that the fracture gradient

increases as the formation pore pressure does. A summary of the equations as given by Aadnøy and Looyeh (2011) are listed below:

Hubbert and Willis

$$G_f = \frac{1}{3} \left(\frac{\sigma_v}{d} + 2 \frac{P_o}{d} \right) \quad \text{for Minimum calculated value} \quad 3.12$$

$$G_f = \frac{1}{2} \left(\frac{\sigma_v}{d} + \frac{P_o}{d} \right) \quad \text{for maximum calculated value} \quad 3.13$$

where;

G_f = formation fracture gradient (psi/ft)

σ_v = overburden stress (psi)

d = depth of formation (ft)

P_o = formation pore pressure

Matthews and Kelly

$$G_f = f_e \left(\frac{\sigma_v}{d} - \frac{P_o}{d} \right) + \frac{P_o}{d} \quad 3.14$$

where;

f_e = effective stress coefficient gotten from fracture data of neighboring well.

Pennebaker

$$G_f = f_p \left(\frac{\sigma_v}{d} - \frac{P_o}{d} \right) + \frac{P_o}{d} \quad \text{Type equation here.} \quad 3.15$$

where;

f_p = stress ratio coefficient, a function of Poisson's ratio and deformation.

Eaton

$$G_f = \left(\frac{\nu}{1 - \nu} \right) \left(\frac{\sigma_v}{d} - \frac{P_o}{d} \right) + \frac{P_o}{d} \quad 3.16$$

where;

ν = Poisson's ratio which can range between 0.25 and 0.5

Christman

$$G_f = f_r \left(\frac{\sigma_v}{d} - \frac{P_o}{d} \right) + \frac{P_o}{d} \quad 3.17$$

where;

f_r = stress ratio factor calculated from fracture data.

The Eaton's method is the mostly used in the petroleum industry. The method is possibly the most precise method as it takes into account the changes in Poisson's ratio, pore pressure gradient and overburden stress.

4.0 Fracture Model

In this chapter, a review is done of the inversion method as developed and presented by Bernt S. Aadnøy in his paper Aadnøy (1989). The inversion technique is based on well fracture model and forms a basis of current models used in the petroleum industry.

4.1 Inversion Technique

The model is used to predict the magnitude of the maximum and minimum in-situ stresses and their directions. As shown in Figure 4-1, many wells with different geometry are drilled in an offshore field. The different orientations offered by these directional wells serve as an advantage in the implementation of this technique. The input data for the method are data obtained from Leak-off, tests from different wells, pore pressure, overburden pressure, azimuth and inclination. The data are obtained from the already drilled wells and back calculation is done to determine the in-situ stress of the field formation.

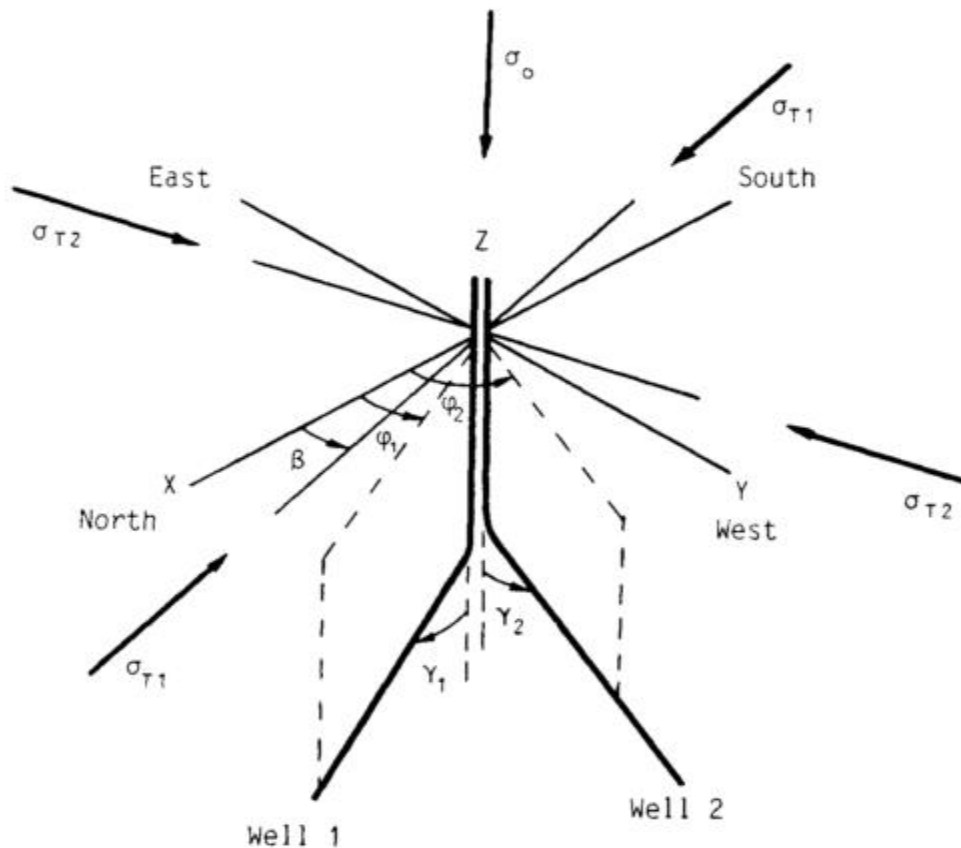


Figure 4-1: Well Geometry

In Figure 4-1, σ_o , σ_{T1} and σ_{T2} are the overburden, maximum and minimum horizontal stresses respectively.

As given by the stress transformation equations in equations 2.38, the principal stresses are given by the following:

$$\begin{aligned}\sigma_1 &= P_w \\ \sigma_2 &= \sigma_z \\ \sigma_3 &= \sigma_\theta\end{aligned}\tag{4.1}$$

Since during hydraulic fracturing, a relationship exists between the tangential stress and the direction of least principal stress, the tangential stress component is therefore, the component of interest. The tangential stress component of equation 2.38 is differentiated with respect to θ and equated to zero in order to solve for the angle θ with reference to the x -axis corresponding to the minimum value of the stress component. The shear stress is considered to have a very small value compared to the normal stresses and hence, neglected. The results of the differentiation represent the maximum and minimum values of the stresses around the wellbore and give angles of: $\theta=0, \pi/2$. Inserting the angles into the tangential stress equation 2.38, the following emerge:

$$\begin{aligned}\sigma_\theta &= 3\sigma_y - \sigma_x - P_w, & \text{for } \theta = 0 \\ \sigma_\theta &= 3\sigma_x - \sigma_y - P_w, & \text{for } \theta = \pi/2\end{aligned}\tag{4.2}$$

Different values are obtained for the normal stresses in the different directions as illustrated in Figure 4-2. At $\theta = 0$, which is the most common case for in-situ stresses, the component of stress in the x -direction is the largest. Conversely, if the largest stress component is in the y -direction, the hole fractures at an angle of $\theta = \pi/2$.

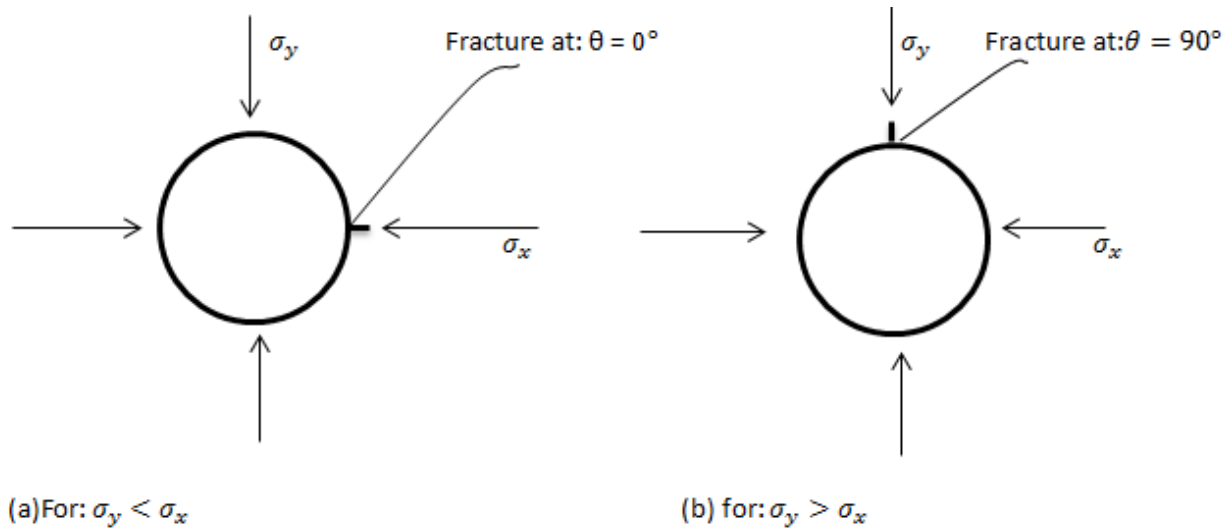


Figure 4-2: Fracture positions on wellbore wall

Fracture can occur at any of the positions as shown in Figure 4-2 depending on the state of stress of the formation. When log information about the fracture traces directions is available, either of the appropriate scenarios can be applied to the stress state. In the event where there is no information about the fracture traces, an assumption is made of the minor and major stress direction, and the model of Figure 4-2(b) is used for critical datasets.

Primarily based on the Kirsch's equations, the well fracture equation is as given by equation 3.11, the fracture equation is in reference to an arbitrarily chosen borehole coordinate system x , y and z and therefore, it is applicable to any wellbore orientation. The equation is derived based on the assumption that $\sigma_x > \sigma_y$. After solving for the values of the maximum and minimum in-situ stresses, the values are put back into the equations to verify that the assumption of $\sigma_x > \sigma_y$ is satisfied. In a situation where the condition is not met, a different equation is used. The equations used are given as follows:

$$P_{wf} = 3\sigma_y - \sigma_x - P_o + \sigma_{tensile} \quad \text{for } \sigma_y < \sigma_x \quad 4.3$$

$$P_{wf} = 3\sigma_x - \sigma_y - P_o + \sigma_{tensile} \quad \text{for } \sigma_y > \sigma_x \quad 4.4$$

Substituting the stress transformation equations from equations 2.36 in the fracture equations 4.3 and 4.4 then rearranging and grouping the known and the unknown the following equations result:

$$\begin{aligned} \frac{P_{wf} + P_o - \sigma_{tensile}}{\sigma_v} + \sin^2\gamma \\ = \{3\sin^2\varphi - \cos^2\varphi\cos^2\gamma\} \frac{\sigma_H}{\sigma_v} \\ + \{3\cos^2\varphi - \sin^2\varphi\cos^2\gamma\} \frac{\sigma_h}{\sigma_v} \end{aligned} \quad 4.5$$

$$\begin{aligned} \frac{P_{wf} + P_o - \sigma_{tensile}}{\sigma_v} - 3\sin^2\gamma \\ = \{3\cos^2\varphi\cos^2\gamma - \sin^2\varphi\} \frac{\sigma_H}{\sigma_v} \\ + \{3\sin^2\varphi\cos^2\gamma - \cos^2\varphi\} \frac{\sigma_h}{\sigma_v} \end{aligned} \quad 4.6$$

Equations 4.5 and 4.6 respectively represent the cases where $\sigma_y < \sigma_x$ and $\sigma_y > \sigma_x$. A critical look at the equations reveals that the only unknown terms are σ_H and σ_h . The equations can be summarized as:

$$P' = a \frac{\sigma_H}{\sigma_v} + b \frac{\sigma_h}{\sigma_v} \quad 4.7$$

where:

for $\sigma_y < \sigma_x$

$$P' = \frac{P_{wf} + P_o - \sigma_{tensile}}{\sigma_v} + \sin^2\gamma$$

$$a = (3\sin^2\varphi - \cos^2\varphi\cos^2\gamma)$$

$$b = (3\cos^2\varphi - \sin^2\varphi\cos^2\gamma)$$

and for $\sigma_y > \sigma_x$

$$P' = \frac{P_{wf} + P_o - \sigma_{tensile}}{\sigma_v} - 3\sin^2\gamma$$

$$a = (3\cos^2\varphi\cos^2\gamma - \sin^2\varphi)$$

$$b = (3\sin^2\varphi\cos^2\gamma - \cos^2\varphi)$$

Inserting the well geometry constants azimuth, φ and inclination, γ , the square terms are resolved and the equations become linear. The linearized equations can be placed in a matrix form and be solved. When many datasets are available from different leak-off tests, the equations can be represented as follows:

$$\begin{bmatrix} P'_1 \\ P'_2 \\ P'_3 \\ \cdot \\ \cdot \\ \cdot \\ P'_n \end{bmatrix} = \begin{bmatrix} a_1 & b_1 \\ a_2 & b_2 \\ a_3 & b_3 \\ \cdot & \cdot \\ \cdot & \cdot \\ \cdot & \cdot \\ a_n & b_n \end{bmatrix} = \begin{bmatrix} \sigma_H/\sigma_v \\ \sigma_h/\sigma_v \end{bmatrix} \quad 4.8$$

and can also be expressed in a simple form as:

$$[P'] = [A][\sigma] \quad 4.9$$

Though, equation 4.9 can be solved with as many datasets as available, a minimum of two datasets are required. The more the datasets used, the better the results obtained. When many datasets are used to solve for only the two unknowns, the equation would result in an over-determined system of linear equations. An exact solution cannot be obtained from the resolution of the over-determined system. The error, that is, the difference between the measured datasets and the model solution is minimized using the least square method for the unknown values to converge to accurate values. The equation for the determination of the error is given as:

$$[e] = [A][\sigma] - [P'] \quad 4.10$$

using the least square method, the error is squared and can be written as:

$$e^2 = [e]^T[e] \quad 4.11$$

In order to minimize the squared error, equation 4.11 is differentiated with respect to $[\sigma]$ and equated to zero as shown below:

$$\frac{\partial e^2}{\partial [\sigma]} = 0 \quad 4.12$$

Substituting equation 4.10 into equation 4.12 and solving the matrices, the maximum and minimum in-situ stresses can be calculated with the following equations:

$$[\sigma] = \{[A]^T[A]\}^{-1}[A]^T[P'] \quad 4.13$$

A computer program is required to solve equation 4.13. The equation is a simple tool to use but complex to be manually resolved. The unknown horizontal in-situ stresses and squared error are calculated with directions all around the wellbore from 0 to 360 degrees. The angle where the error is smallest gives the directions of the in-situ stresses and the corresponding magnitudes.

However, the challenge here is that the direction obtained, β is in relation to an arbitrarily chosen coordinate system as shown in Figure 4-1, where; X and Y coordinates are perpendicular to each other and directed in the horizontal plane, Z is directed in the vertical plane. But, of interest to us are the directions of the in-situ stresses in relation to the known well geometry. In order, to capture this properly, β is introduced into the equation and the following steps are taken:

$$[A] = \begin{bmatrix} a_1 & b_1 \\ a_2 & b_2 \\ a_3 & b_3 \\ \cdot & \cdot \\ \cdot & \cdot \\ \cdot & \cdot \\ a_n & b_n \end{bmatrix} \quad 4.14$$

where:

for $\sigma_y < \sigma_x$, $i = 2, 3, \dots, n$

$$\begin{aligned} a_i &= 3\sin^2(\varphi_i - \beta) - \cos^2(\varphi_i - \beta)\cos^2\gamma_i \\ b_i &= 3\cos^2(\varphi_i - \beta) - \sin^2(\varphi_i - \beta)\cos^2\gamma_i \end{aligned} \quad 4.15$$

and for $\sigma_y > \sigma_x$

$$\begin{aligned} a_i &= 3\cos^2(\varphi_i - \beta)\cos^2\gamma - \sin^2(\varphi_i - \beta) \\ b_i &= 3\sin^2(\varphi_i - \beta)\cos^2\gamma - \cos^2(\varphi_i - \beta) \end{aligned} \quad 4.16$$

The next step to take is to calculate for the horizontal in-situ stresses using:

$$\begin{bmatrix} \overline{\sigma_H} \\ \overline{\sigma_v} \\ \overline{\sigma_h} \\ \overline{\sigma_v} \end{bmatrix} = \{[A]^T [A]\}^{-1} [A]^T [P'] \quad 4.17$$

where:

$$P'_i = \frac{(P_{wfi} + P_{oi} - \sigma_{tensile\ i})}{\sigma_{vi}} + \sin^2\gamma_i \quad 4.18$$

for $\sigma_y < \sigma_x$ $i = 2, 3, \dots, n$ and for $\sigma_y > \sigma_x$:

$$P'_i = \frac{(P_{wfi} + P_{oi} - \sigma_{tensile\ i})}{\sigma_{vi}} - 3\sin^2\gamma_i \quad 4.19$$

In the final step, the squared error is computed from the equation 4.11. The whole process is repeated again for the angles round the borehole, that is β is varied as $0^\circ \leq \beta \leq 360^\circ$. The squared error is plotted against the values of β and the minimum value corresponds to the horizontal in-situ stress direction relative to X-direction. At that same angle β the magnitude of the horizontal in-situ stresses are obtained. It is also important to note that the tensile strength of the rock formation is assumed to be equal to zero, except where very credible fracture data is available.

With the determination of the horizontal in-situ stresses and direction, the fracture pressure of a future well can easily be made. This is done by introducing β into σ_x and σ_y of equation 2.36 and substituting into fracture equations 4.3 and 4.4. The resulting equations are:

for $\sigma_y < \sigma_x$

$$P_{wf} = 3(\sigma_H \sin^2(\varphi - \beta) + \sigma_h \cos^2(\varphi - \beta)) - \{(\sigma_H \cos^2(\varphi - \beta) + \sigma_h \sin^2(\varphi - \beta)) \cos^2 \gamma + \sigma_v \sin^2 \gamma\} - P_o \quad 4.20$$

and for $\sigma_y > \sigma_x$

$$P_{wf} = 3\{(\sigma_H \cos^2(\varphi - \beta) + \sigma_h \sin^2(\varphi - \beta)) \cos^2 \gamma + \sigma_v \sin^2 \gamma\} - (\sigma_H \sin^2(\varphi - \beta) + \sigma_h \cos^2(\varphi - \beta)) - P_o \quad 4.21$$

4.2 Other models used

In this section, other fracture models that are currently in used are presented briefly. Some of the models are modifications of the conventional inversion technique as presented above while others are entirely based on different theories. Over the years, various authors have proposed different models and claimed that their model give a better result, yet, no single model has been universally accepted. It is not the aim of this thesis to exhaust the list of models, hence, only a few would be discussed here.

Thorsen (2011) proposed a method to determine the in-situ stresses using wellbore failure. In his approach, he made use of the extended linear principal stress failure and linear elasticity. The extended failure criterion is based on the theory that a general class form can be used to represent all failure criteria. This ensure more flexibility and the choice of failure criterion can be left until a later stage when there are more information to select the appropriate criterion. By assuming that for a formation to fracture or to collapse the maximum principal stress that result to fracture is the same as the minimum principal stress required for collapse which is $\sigma_r = P_w$, he gave the function for the extended linear principal stress failure as:

$$L = f(P_w) + (c_1\sigma_\theta + c_2\sigma_z)\cos^2\alpha + (c_1\sigma_z + c_2\sigma_\theta)\sin^2\alpha + (c_1 - c_2)\sigma_{\theta z}\sin 2\alpha = 0 \quad 4.22$$

where:

P_w is the well pressure, L is the corresponding failure function class and a failure criterion applied at $L=0$, f is a general function that either depends on principal stress or not dependent on stress state. c_1 and c_2 are constants that depend on material properties.

Equation 4.22 is satisfied at failure initiation point when $\theta = \theta_f$ and $P_w = P_{wf}$ at failure initiation pressure. At failure initiation, L is at maximum. Differentiating L with respect to θ and α :

$$\begin{aligned} \partial_\theta L = 2\{ & [(c_1 + c_2)(1 + \nu) + (c_1 - c_2)(1 - \nu)\cos 2\alpha] \\ & \times [(\sigma_x - \sigma_y)\sin 2\theta - 2\sigma_{xy}\cos 2\theta] \\ & - (c_1 - c_2)\sin 2\alpha(\sigma_{xz}\cos\theta + \sigma_{yz}\sin\theta)\} = 0 \end{aligned} \quad 4.23$$

$$\partial_\alpha L = (c_1 - c_2)[2\sigma_{\theta z}\cos 2\alpha + (\sigma_z - \sigma_\theta)\sin 2\alpha] = 0 \quad 4.24$$

Combining equations 4.22, 4.23 and 4.24 with the principal in-situ stresses and after some manipulations a result in the following form is obtained:

$$a_H\sigma_H + a_h\sigma_h = a_f \quad 4.25$$

where a is a function of wellbore orientation, orientation of principal in-situ stress, Poisson's ratio, failure data $(\theta_f, P_{wf}, \alpha)$ and the failure criterion constants (f, c_1, c_2) . Detailed derivations can be found in his paper Thorsen (2011). The equations can then be resolved using the inversion technique and least square method to determine the magnitude of the principal in-situ stresses.

In their paper, Zhang et al. (2013) proposed a modified version of the Inversion technique as given by Aadnoy (1989) and presented here in section 4.1. They added a new feature to

accommodate the effect of reservoir production history in the determination of the in-situ stresses and claimed that the changes in pore pressure introduced in the model increases the accuracy. The theory of poroelasticity, which shows that the stress in the reservoir is affected by the pore pressure, is then used to compute the reservoir horizontal stresses for each of the pore pressure. The in-situ stresses in the reservoir for each of the pore pressure are predicted using the orthotropic rock model and the poroelasticity theory. The proposed equations for the determination of the horizontal minimum and maximum in-situ stresses are:

$$\sigma_h = \Gamma v_{vmin} + \Gamma v_h v_{vmax} - \beta P_o \quad 4.26$$

$$\sigma_H = \Gamma v_h v_{vmin} + \Gamma v_{vmax} - \beta P_o \quad 4.27$$

in which:

$$\Gamma = \left(\frac{1}{1 - v_h^2} \right) (\sigma_v + \beta P_o)$$

The Poisson's ratios v_{vmax} and v_{vmin} in the direction of the maximum and minimum horizontal stress components are obtained by substituting equations 4.26 and 4.27 into the general fracture equation 4.5 to give the following equations:

$$\begin{aligned} & \frac{P_{wf} + P_o + (a + b)\beta P_o - \sigma_{tensile}}{\sigma_v} + \sin^2 \gamma \\ & = \frac{\Gamma(a \cdot v_h + b)}{\sigma_v} v_{vmin} + \frac{\Gamma(a + b \cdot v_h)}{\sigma_v} v_{vmax} \end{aligned} \quad 4.28$$

Similarly, equation 4.8 becomes:

$$\begin{bmatrix} P'_1 \\ P'_2 \\ \cdot \\ \cdot \\ P'_n \end{bmatrix} = \begin{bmatrix} A_1 & B_1 \\ A_2 & B_2 \\ \cdot & \cdot \\ \cdot & \cdot \\ A_n & B_n \end{bmatrix} \begin{bmatrix} v_{vmin} \\ v_{vmax} \end{bmatrix} \quad 4.29$$

where:

$$P'_i = \frac{P_{wfi} + P_{oi} + (a_i + b_i)\beta P_{oi} - \sigma_{tensile}}{\sigma_{vi}} + \sin^2\gamma_i$$

$$A_i = \frac{\Gamma_i(a_i \cdot v_h + b_i)}{\sigma_{vi}}$$

$$B_i = \frac{\Gamma_i(a_i + b_i \cdot v_h)}{\sigma_{vi}}$$

Similarly, with two unknowns, equation 4.29 is solved for an over determined system and using the least square approach. Details of the derivations and utilization of the equations can be found in the publication Zhang et al. (2013).

While the methods discussed above proposed techniques to estimate the maximum and minimum horizontal in-situ stresses, some authors maintain that the minimum in-situ stress can be directly measured from hydraulic fracturing test. The argument is based on the premise that when there is a break in a link, it is the weakest link that breaks and hence, one can only identify the weakest link and not the strongest link. Though, procedures and methods may differ but Zoback and Haimson (1982), Kunze and Steiger (1992), and Raaen et al. (2001) all agree that data from hydraulic fracturing test can accurately give the magnitude of the minimum horizontal principal in-situ stress.

5.0 Computer Data Program

5.1 Introduction

The programming language used here is Matlab. Matlab was chosen because it is a very powerful mathematical tool for dealing with matrices and arrays and in addition to its robustness, accessibility, availability, easy to learn and use. Its codes can also easily be converted to other computer languages. Matlab has a large user base and promises to be a useful tool in the distant future.

The primary objective of the program is to estimate the magnitude of the maximum and minimum horizontal in-situ stresses and their corresponding directions from LOT data. The program is simple, flexible but very powerful and designed to achieve the objective with three major steps. The steps are as follows:

1. Modelling
2. Quality check
3. Prognosis

5.2 Modelling

The heart of the program is developed based on the model presented in 4.1 Inversion Technique. A minimum of 3 datasets are required to get a good result. Due to the uncertainties in the state of stress of the formation, the model runs every dataset with both equations 4.5 and 4.6. In the program, the mode [0] is used to represent when equation 4.5 is applied and mode [1] when equation 4.6 is used. For every given dataset all possible combinations are run. The total number of combination of runs in any case is given by 2^n , where n is the number of datasets to be tested. For instance, for a three datasets test, the program would have solutions for 8 different combinations. Due to symmetry, the in-situ stresses, the squared error, stress difference ($\sigma_x - \sigma_y$) and β are calculated 180 times ($0 \leq \beta \leq 180$) instead of 360 times. For every computation the program tests the result to certify that $\sigma_y < \sigma_x$ if equation 4.5 or $\sigma_y > \sigma_x$ if equation 4.6 is used. Out of these solutions, based on the least square method and the mode of equation used, the program eliminates the combinations with unrealistic solution and the combination that gives the best solution is selected. The program displays the values of the estimated in-situ stresses and β direction. A soft copy of the program is included and the codes are placed in the appendix.

5.3 Quality Check

The selected solution is verified by inserting the values of the estimated in-situ stresses and β into the fracture equations of 4.3 and 4.4 making use of equations 4.15 and 4.16. The program displays the estimated fracture pressure for the user's inspection and direct comparison with the formation fracture pressure obtained from the measured data.

5.4 Prognosis

When a future well is planned with some known information such as the azimuth, inclination, overburden stress and pore pressure, the program is designed to predict the fracture pressure of the proposed well. The prediction is based on the estimated maximum and minimum horizontal in-situ stresses and the direction β obtained from the model. Equations 4.20 and 4.21 are used for these computations.

5.5 User guide

The program is easy to use as input data in the Matlab graphic user interface is reduced to a minimum. The user must have Matlab installed as a platform to run the program. Along with the program is an excel sheet where the user can capture all the necessary data gotten from the hydraulic fracture tests. For the program to run successfully the following steps should be followed:

Step 1

Open and populate the excel file 'Inv.xlsx' with measured data under the following headings as shown in Figure 5-1. Dataset is a serial number of the datasets, Pwf is the fracture gradient, Po is formation pore pressure, Ov is Overburden, Inc is inclination and Az is the azimuth.

In-Situ stress measurement from LOT data using Inversion method


Dataset	Pwf	Po	Ov	Inc	Az
1	1.53	1.03	1.71	0	27
2	1.84	1.39	1.81	27	92
3	1.82	1.53	1.89	35	92
4	1.47	1.03	1.71	23	183
5	1.78	1.25	1.82	42	183
6	1.87	1.57	1.88	41	183
7	1.49	1.03	1.71	23	284
8	1.64	1.05	1.78	48	284
9	1.84	1.53	1.88	27	284
10	0	1.03	1.71	15	135
11	0	1.19	1.8	30	135
12	0	1.55	1.89	45	135
14					

Figure 5-1: Data Capture Sheet

Datasets 10, 11 and 12 are for the future wells, input zeroes (0) for the values of the unknown Pwf. If the intention of the user is not to predict the Pwf of proposed well or no available information, the rows can be left out altogether.

The file should then be saved in the location 'C:\temp\Inv.xlsx'. It is very important that the file maintains the given address, the Matlab program default state is to read the data from this directory. In the event that the excel file is located elsewhere, the 'Search for datafile' button in the graphic user interface in Figure 5-2 can be used to locate the file. The user must ensure that the complete address is captured. At any time, the user can open the excel file and change the input data as required.

Step 2

Copy and save in one location the other 3 files: Inversion_Method.fig, Inversion_Method.m and Inversion_Technique.m. These files can be saved anywhere in the system, for example, save files in C:\Users\Documents\MATLAB. Open the Inversion_Method.m file and click the run button  in the editor tab. It will bring up the graphic user interface as shown in Figure 5-2. Ensure that

the address displayed is the location of the excel file, if not, Search for the excel file and press enter for the ‘Dataset’ and ‘Dataset + Prognosis’ columns to populate. For the first selection ‘Dataset’, select the combination of datasets to be tested. Selection is done by pressing the **Ctrl** key down and clicking to select or deselect (Figure 5-3). In the second selection ‘Prognosis + Datasets’, select the same datasets as the first selection and also in addition the dataset to be predicted. In the case where the prognosis is not of interest, the second datasets selection should be exactly the same as the first selected datasets.

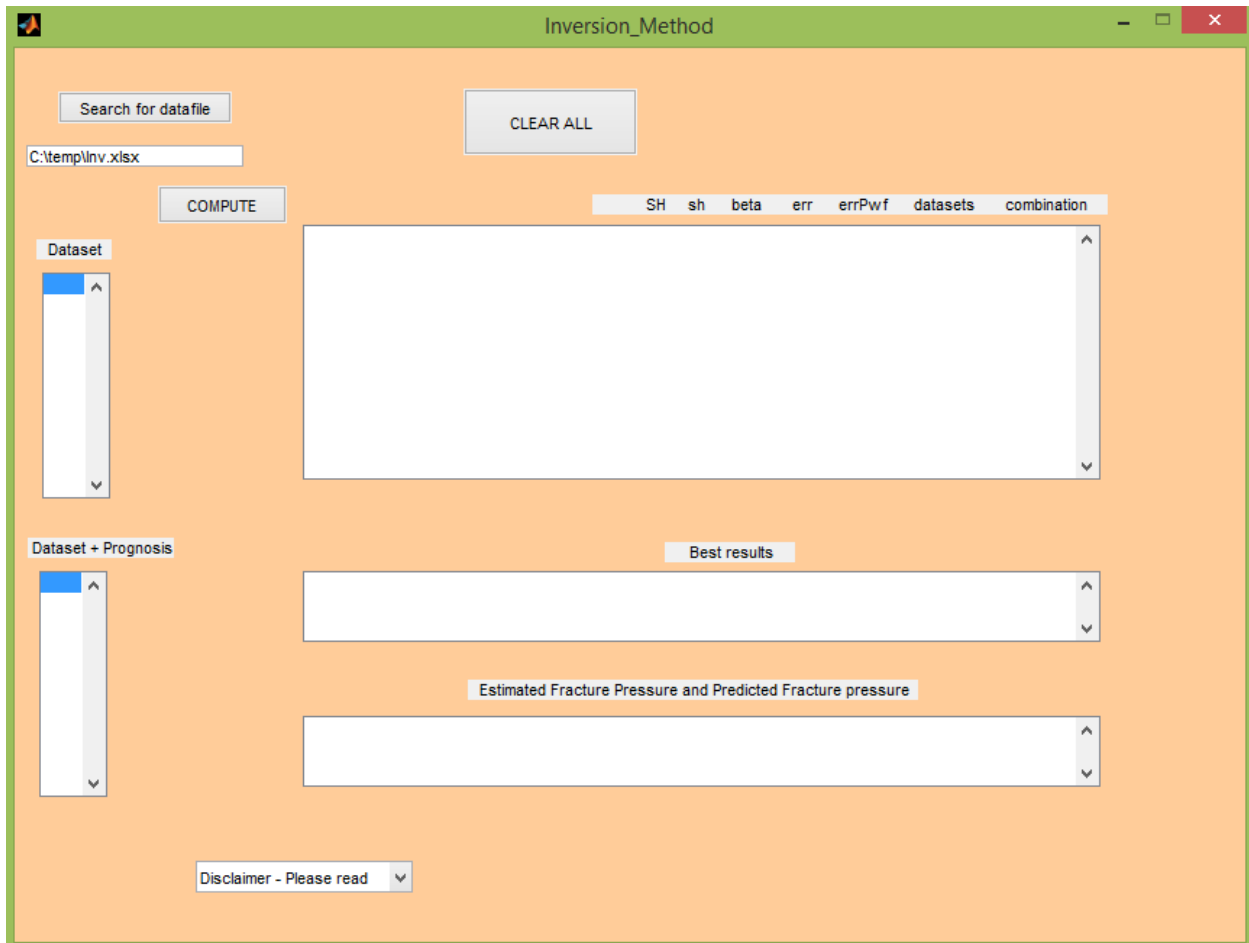


Figure 5-2: Graphic User Interface Layout

Step 3

Run the program by pressing the pushbutton ‘COMPUTE’. The results output is as given in Figure 5-3. ‘SH’ is the ratio of the maximum horizontal stress to the overburden stress, ‘sh’ is the ratio of the minimum horizontal stress to the overburden stress, ‘beta’ is the β angle in degrees,

In-Situ stress measurement from LOT data using Inversion method

‘err’ is the minimum squared error, ‘errPwf’ is the difference between the measured fracture pressure and the estimated fracture pressure, ‘datasets’ is the selected datasets for computation and ‘combination’ is the combination of the equations used. ‘Best results’ give the best solution combinations with the least error. ‘Estimated Fracture Pressure and Predicted Fracture Pressure’ displays the computed fracture pressure of the selected datasets and if applicable the prognosis fracture pressure (not applicable in this example).

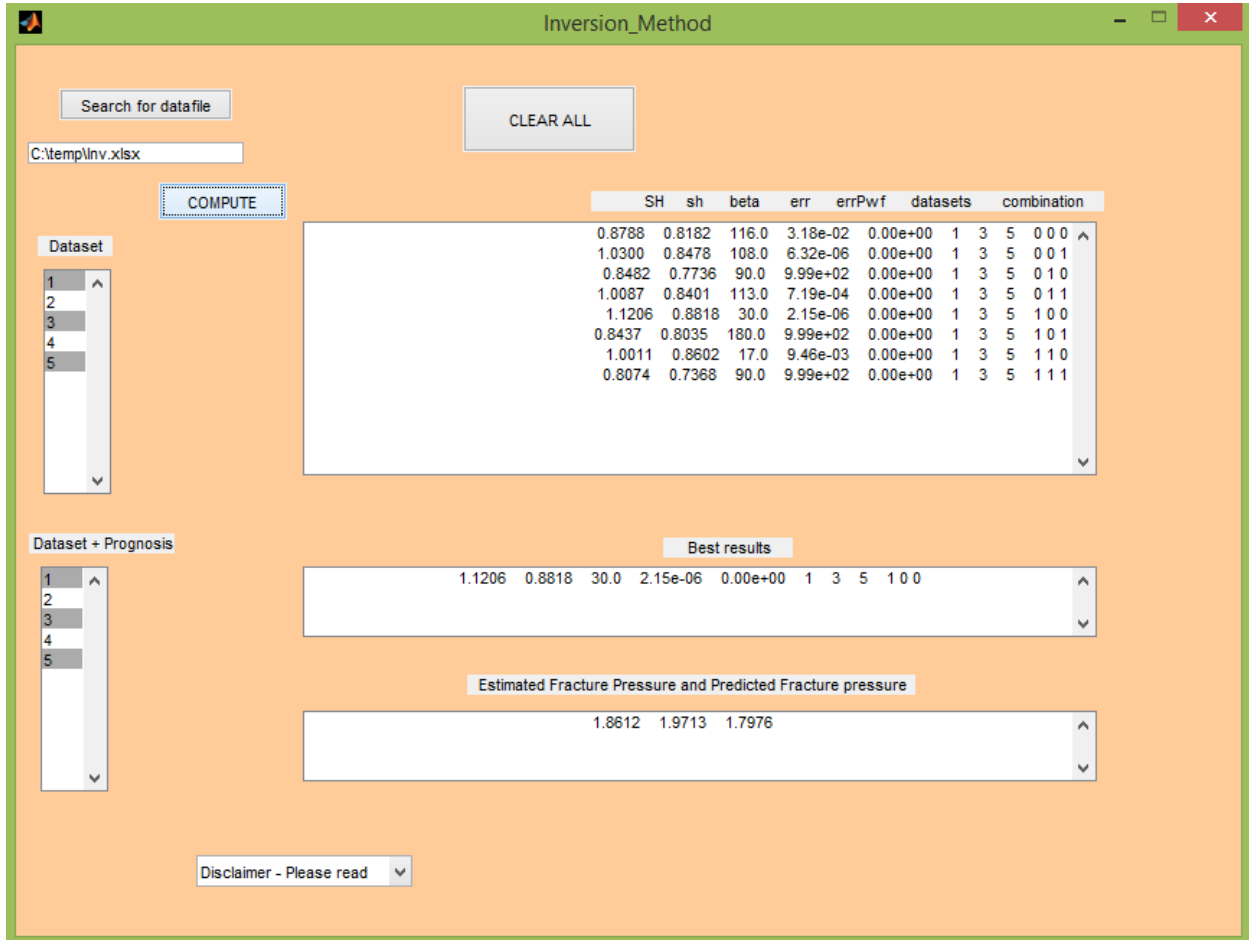


Figure 5-3: Graphic User Interface Results Output

The ‘CLEAR ALL’ button clears all stored results before the next run.

6.0 Field cases, simulation and discussion of results

In this chapter, fracture tests data from two different fields are presented. Based on the well fracture data, simulations are done and the results are analyzed. Two different Field cases are simulated to illustrate the robustness of the tool.

Field case 1

To demonstrate the efficacy of the tool, a field case with real data is simulated to determine the state of stress of the field. The LOT data were obtained from the Snorre field in the North Sea (Djurhuus, 2002). Three wells, P-7, P-8 and P-9 are considered for this test. The depths of the wells range from about 700 to 2400 meters and are presented in Table 4. Simulations are done here to determine the in-situ stresses and the obtained values are used to compute the fracture pressures.

Table 4: Fracturing data for Field case 1

Data set	Well	Casing (in)	D (m)	P_{wf} (s.g.)	P_o (s.g.)	σ_v (s.g.)	γ (°)	φ (°)
1	P-7	18 5/8	1160	1.44	0.9767	1.8481	19.37	196.92
2	P-7	13 3/8	1774	1.71	1.3993	1.9649	70.63	195.90
3	P-7	9 5/8	2369	1.87	1.3814	2.0511	60.56	220.76
4	P-8	18 5/8	756	1.39	0.9483	1.7325	8.61	167.78
5	P-8	13 3/8	1474	1.65	1.2213	1.9151	60.26	187.65
6	P-8	9 5/8	2321	1.83	1.3789	2.0475	43.82	129.16
7	P-9	18 5/8	1005	1.59	0.9685	1.8087	16.88	92.77
8	P-9	13 3/8	1503	1.62	1.2568	1.9199	36.30	85.69
9	P-9	9 5/8	2418	1.75	1.3840	2.0548	55.09	89.13

Simulation 1

A simulation of all datasets (1,2,3,4,5,6,7,8,9) is run for all possible combinations around the wellbore (360 degrees) to determine state of stress, based on the minimum squared error as shown in Figure 6-1, the most suitable solution is selected and given as:

$$\sigma_H/\sigma_v = 1.3392$$

$$\sigma_h/\sigma_v = 0.8356$$

$$\beta = 104^\circ$$

$$\text{Squared error} = 0.1027$$

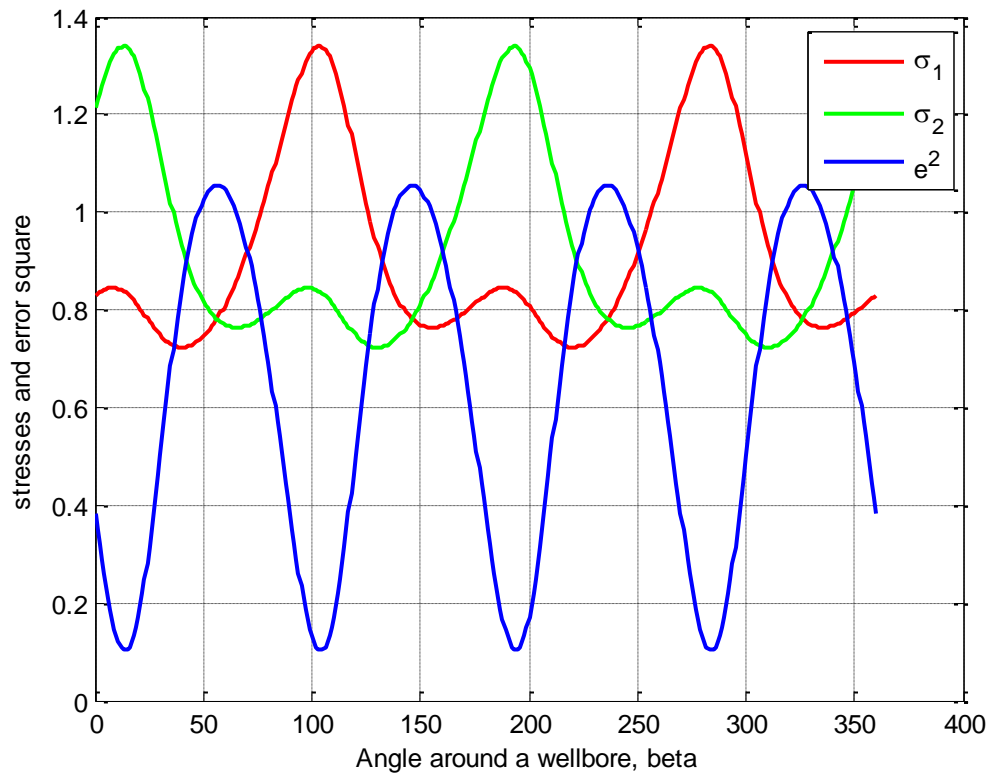


Figure 6-1: In-situ stresses and error squared around the wellbore case 1, simulation 1.

The results given for the horizontal stresses ratio show that the maximum horizontal principal in-situ stress is 1.3392 times the overburden, the minimum horizontal stress is 0.8356 times the

overburden and the angle beta gives the direction of the maximum in-situ stress with reference to the North. The error is too large. To check how these results correlate with the input data, the model fracture pressures are then computed to enable comparison with the measured data. The results are tabulated below:

Table 5: Comparison of the measured and estimated fracture pressure of Case 1, Simulation 1

Datasets	Measured $P_{wf}(s.g)$	Estimated $P_{wf}(s.g)$
1	1.44	1.29
2	1.71	1.76
3	1.87	2.14
4	1.39	1.76
5	1.65	1.75
6	1.83	2.00
7	1.59	1.33
8	1.62	1.56
9	1.75	1.71

According to Aadnoy and Looyeh (2011) the difference between the measured and predicted fracture pressure should be in the range of 0.05 to 0.10 s.g. The results from the model do not match the test data as shown in Table 5, this signify that the simulated datasets do not accurately represent the state of stress of the entire field depth. To get a better representation of the stress state of the field, simulations are done in smaller areas.

Simulation 2

A second simulation run is carried out with datasets 1, 4 and 7. These datasets are associated with the 18 5/8 in casing shoe. The following results were obtained:

$$\sigma_H/\sigma_v = 0.7088$$

$$\sigma_h/\sigma_v = 0.6825$$

$$\beta = 12^\circ$$

Squared error = 0.0000

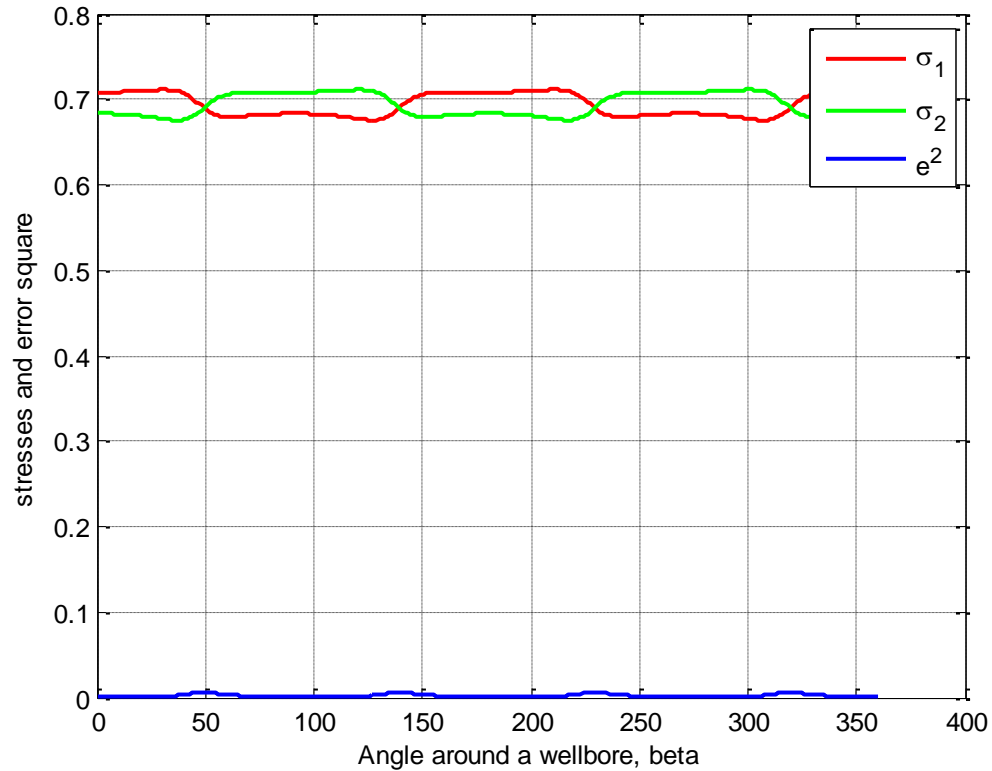


Figure 6-2: In-situ stresses and error squared around the wellbore case 1, simulation 2

The error from the second simulation is zero, indicating very good stress ratio values. To further validate the results, the estimated fracture pressures are then computed. The modelled fracture pressures as compared with the measured data are captured below:

Table 6: Comparison of the measured and estimated fracture pressure of Case 1, simulation 2

Datasets	Measured $P_{wf}(s.g)$	Estimated $P_{wf}(s.g)$
1	1.44	1.44
4	1.39	1.39
7	1.59	1.59

The results of the second simulation give a perfect match with that of the measured data which is an indication of a good appraisal of the stress fields around the depth region of the 18 5/8 casing shoe which ranges from about 700m to 1200m.

Simulation 3

A third simulation is again run with datasets 2, 5 and 8 representing data from each well at the 13-3/8 in casing shoe. The results obtained are:

$$\sigma_H / \sigma_v = 1.5864$$

$$\sigma_h / \sigma_v = 0.9458$$

$$\beta = 78^\circ$$

$$\text{Squared error} = 0.0000$$

Table 7: Comparison of the measured and estimated fracture pressure of Case 1, simulation 3

Datasets	Measured P_{wf} (s.g)	Estimated P_{wf} (s.g)
2	1.71	1.71
5	1.65	1.65
8	1.62	1.62

These datasets also give a perfect match between the predicted fracture pressure and the measured data representing a very good assessment of the state of stress at the depth level.

Simulation 4

A final simulation is done to determine the state of stress around the 9 5/8 in casing shoe. The datasets 3, 6 and 9 are simulated and calculated results are given below:

In-Situ stress measurement from LOT data using Inversion method

$$\sigma_H / \sigma_v = 0.8542$$

$$\sigma_h / \sigma_v = 0.8238$$

$$\beta = 104^\circ$$

$$\text{Squared error} = 0.0000$$

Table 8: Comparison of the measured and estimated fracture pressure of Snorre field

Well	Measured $P_{wf}(s.g)$	Estimated $P_{wf}(s.g)$
3	1.87	1.87
6	1.83	1.83
9	1.75	1.75

The estimated horizontal in-situ stresses ratio give a good account of the state of stress at the depth level of the Snorre field. The results are validated by the modelled fracture pressures which give a perfect match with the measured data.

Field Case 2

Aadnoy and Looyeh (2011) presented a field case with three drilled wells and a plan to drill the fourth well. To visualize the scenario, vertical and horizontal projections of the wells are presented in Figure 6-3. and Figure 6-4. In this case, a new well is to be drilled and prognosis is made to give an estimate of the fracture pressure of the new well based on the modelled in-situ stresses. Presented in Table 9 are measured data.

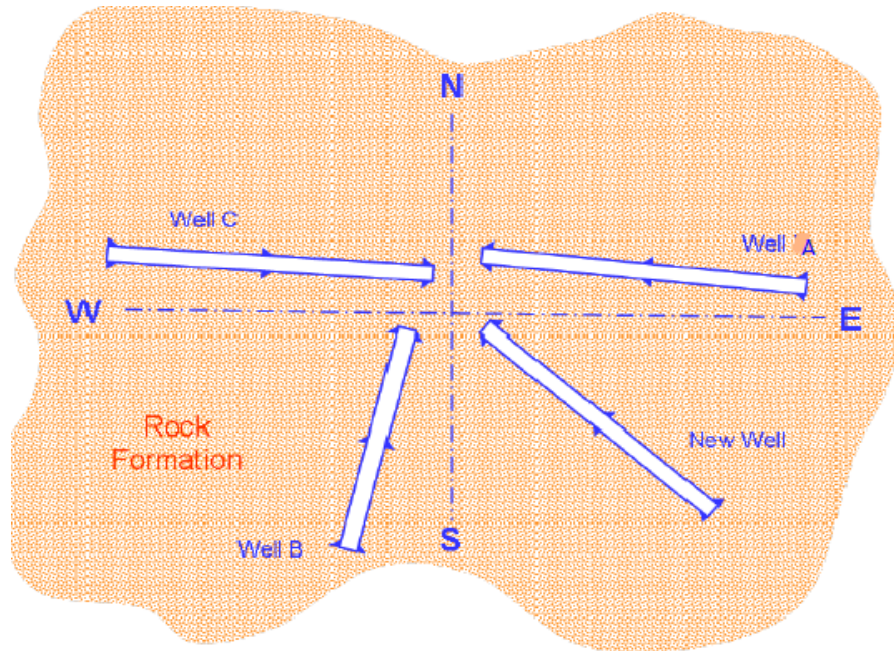


Figure 6-3: Horizontal view of well

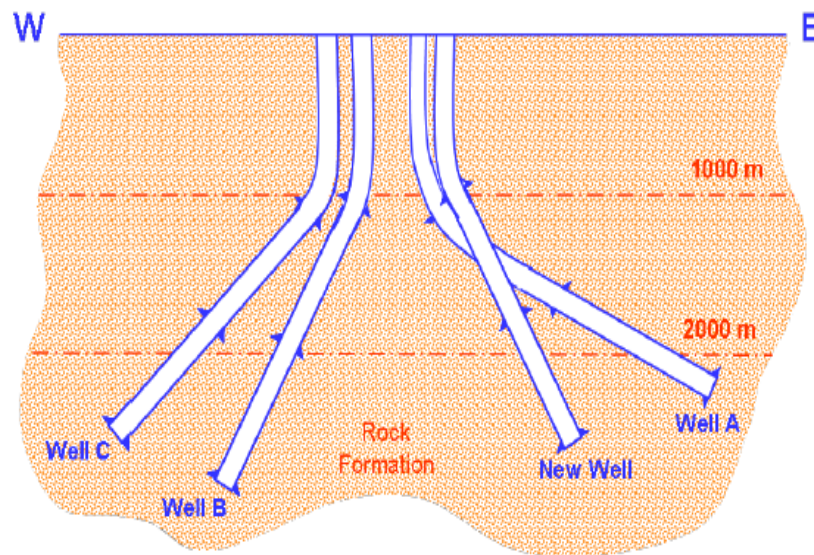


Figure 6-4: Vertical view of well

Table 9: Fracturing data for Field case 2

Data set	Well	Casing (in)	TVD(m)	$P_{wf}(s.g.)$	$P_o(s.g.)$	$\sigma_v(s.g.)$	$\gamma(^{\circ})$	$\varphi(^{\circ})$
1	A	20	1101	1.53	1.03	1.71	0	27
2		13-3/8	1888	1.84	1.39	1.81	27	92
3		9-5/8	2423	1.82	1.53	1.89	35	92
4	B	20	1148	1.47	1.03	1.71	23	183
5		13-3/8	1812	1.78	1.25	1.82	42	183
6		9-5/8	2362	1.87	1.57	1.88	41	183
7	C	20	1141	1.49	1.03	1.71	23	284
8		13-3/8	1607	1.64	1.05	1.78	48	284
9		9-5/8	2320	1.84	1.53	1.88	27	284
10	New	20	1100	-	1.03	1.71	15	135
11		13 3/8	1700	-	1.19	1.80	30	135
12		9 5/8	2400	-	1.55	1.89	45	135

Simulation 1

As in previous cases, a simulation of all available datasets is run to get an average stress of the formation. For datasets 1 – 9, the estimated results are:

$$\sigma_H/\sigma_v = 0.9749$$

$$\sigma_h/\sigma_v = 0.7711$$

$$\beta = 141^{\circ}$$

$$\text{Squared error} = 0.14$$

Table 10: Comparison of the measured and estimated fracture pressure of Case 2, simulation 1

Datasets	Measured P_{wf} (s. g.)	Estimated P_{wf} (s. g.)
1	1.53	1.49
2	1.84	1.82
3	1.82	1.79
4	1.47	1.85
5	1.78	1.76
6	1.87	1.54
7	1.49	1.74
8	1.64	1.76
9	1.84	1.50

The significant difference between the fracture pressures from the test and the calculated fracture pressures as shown in the comparison in Table 10 clearly illustrate that a simulation of these datasets covering large area does not accurately describe the stress state of the formation. To get a better picture of the state of stress, simulation is done in small sections.

Simulation 2

The second simulation is done with data taken after the installation of the surface casing, from Table 9, data 1,4, 7 and 10 are associated with the 20-in casing shoe. Running the simulation with the known 1, 4 and 7 give the following in-situ stresses ratio:

$$\sigma_H / \sigma_v = 0.7543$$

$$\sigma_h / \sigma_v = 0.7505$$

$$\beta = 27^\circ$$

To validate these results, the predicted fracture pressures are computed. A prediction is also made for the new well, dataset 10.

Table 11: Comparison of the measured and estimated fracture pressure of Case 2, simulation 2

Datasets	Measured P_{wf} (s.g.)	Estimated P_{wf} (s.g.)
1	1.53	1.53
4	1.47	1.47
7	1.49	1.49
10	–	1.53

From the results, it shows that the stresses obtained accurately represent the stress state of the formation around the depth of the 20-in casing shoe. In addition, fracture pressure for the new well is computed. This is very useful as it gives the driller an upper window when drilling in order not to fracture the formation. Simulations are done for the other casing shoes, to determine the state of the stresses at the regions. Some of the datasets combination best results gave non-realistic or unmatched values, such combinations are discarded. In such cases, one model is not sufficient to appropriately represent the stress state of the selected data sets.

Like all numerical analysis problem, there is the possibility of more than one possible solution. It is even very close here because the simulation is done around the wellbore with a step of 1°, making the computed results very close to call. Out of the possible solutions, as shown in Figure 5-3, the program picks the one with the smallest error as the best solution. The results obtained from the simulations of the two field cases show remarkable accuracy and correlation.

The results also show that a single simulation cannot be used to map out the stress state of an entire field as shown by the variation of stresses with depth.

According to Aadnoy et al. (1994), many faults are observed in the Snorre field but the predominant is the normal faulting. The results obtained from the Snorre field is in agreement with this as we see that the stress ratio obtained in simulation 1 and 3 satisfy the conditions of effects of faulting and bounds on in-situ stress as presented in chapter 2.

7.0 Summary and Conclusion

Accurately predicting the in-situ stresses in a rock formation can go a long way to solve a lot of the challenges facing the petroleum and mining industries and a whole lot of money could be saved and accidents averted. In this thesis, a handy tool that is easy to use to predict the horizontal principal in-situ stresses was developed. The results from simulations obtained from this work demonstrated the accuracy and ability of this program to:

1. Estimate the magnitude and direction of the horizontal principal in-situ stresses of a rock field based on data obtained from LOT, pore pressures, overburden stresses and well directions. The model can accommodate any number of input data but a minimum of three input data is required to get a meaningful result.
2. Validate the results by calculating the fracture pressures based on the computed in-situ stresses for the user to have a direct comparison with the measure data from the test.
3. Predict the fracture pressures of a future well based on calculations derived from LOT data from previously drilled well.

It is recommended that this tool is used as a guide when planning well and field development; it can be used alongside other commercial software.

References

- AADNØY, B. & LOOYEH, R. 2011. *Petroleum Rock Mechanics: Drilling Operations and Well Design*, Boston, Gulf Professional Publishing.
- AADNOY, B. S. 1989. Inversion Technique To Determine the In-Situ, Stress Field From Fracturing Data. Society of Petroleum Engineers.
- AADNØY, B. S. 2010. *Modern Well Design*, The Netherlands, CRC Press/Balkema.
- AADNOY, B. S., BRATLI, R. K. & LINDHOLM, C. D. 1994. In-situ stress modelling of the Snorre field. Society of Petroleum Engineers.
- AADNOY, B. S. & CHENEVERT, M. E. 1987. Stability of Highly Inclined Boreholes (includes associated papers 18596 and 18736).
- AADNOY, B. S. & HANSEN, A. K. 2005. Bounds on In-Situ Stress Magnitudes Improve Wellbore Stability Analyses. *Society of Petroleum Engineers*.
- AADNOY, B. S., KAARSTAD, E. & GONSALVES, C. J. D. C. 2013. Obtaining Both Horizontal Stresses from Wellbore Collapse. Society of Petroleum Engineers.
- AADNOY, B. S. & LOOYEH, R. 2011. *Petroleum Rock Mechanics: Drilling Operations and Well Design*.
- ADDIS, M. A., HANSSEN, T. H., YASSIR, N., WILLOUGHBY, D. R. & ENEVER, J. 1998. A Comparison Of Leak-Off Test And Extended Leak-Off Test Data For Stress Estimation. Society of Petroleum Engineers.
- ALAM, M. M., FABRICIUS, I. L., HJULER, M. L. & CHRISTENSEN, H. F. 2012. Influence of Effective Stress Coefficient On Mechanical Failure of Chalk. American Rock Mechanics Association.
- ALTUN, G., LANGLINAIS, J. & BOURGOYNE, A. T., JR. 1999. Application of a New Model to Analyze Leakoff Tests. Society of Petroleum Engineers.
- BAI, M. 2011. Risk And Uncertainties In Determining Fracture Gradient And Closure Pressure. American Rock Mechanics Association.
- CARNEGIE, A., THOMAS, M., EFNİK, M. S., HAMAWI, M., AKBAR, M. & BURTON, M. 2002. An Advanced Method of Determining Insitu Reservoir Stresses: Wireline Conveyed Micro-Fracturing. Society of Petroleum Engineers.
- CHRISTMAN, S. A. 1973. Offshore Fracture Gradients. *Journal of Petroleum Technology*.
- DJURHUUS, J. 2002. Analytical investigation of in-situ stresses and hydraulic induced borehole fractures Ph.D Thesis, University of Faroe Islands

In-Situ stress measurement from LOT data using Inversion method

- EATON, B. A. 1969. Fracture Gradient Prediction and Its Application in Oilfield Operations. *Society of Petroleum Engineers*.
- FJÆR, E., HOLT, R. M., HORSRUD, P., RAAEN, A. M. & RISNES, R. 2008. *Petroleum Related Rock Mechanics*, Elsevier Science.
- HUBBERT, M. K. & WILLIS, D. G. 1957. Mechanics Of Hydraulic Fracturing. Society of Petroleum Engineers.
- KUNZE, K. R. & STEIGER, R. P. 1992. Accurate In-Situ Stress Measurements During Drilling Operations. Society of Petroleum Engineers.
- LOUDEN, L. R. 1972. Origin and Maintenance of Abnormal Pressures. Society of Petroleum Engineers.
- NGUYEN, T. 2013. Compedium on Well Design. Available: http://infohost.nmt.edu/~petro/faculty/Nguyen/PE413/Presentation/C1/2_FracturePressure.ppt [Accessed 15/04/2014].
- PENNEBAKER, E. S. 1968. An Engineering Interpretation of Seismic Data. Society of Petroleum Engineers.
- PEUCHEN, J. & KLEIN, M. 2011. Prediction of Formation Pore Pressures for Tophole Well Integrity. Offshore Technology Conference.
- RAAEN, A. M., HORSRUD, P., KJØRHOLT, H. & ØKLAND, D. 2006. Improved routine estimation of the minimum horizontal stress component from extended leak-off tests. *International Journal of Rock Mechanics and Mining Sciences*, 43, 37-48.
- RAAEN, A. M., SKOMEDAL, E., KJØRHOLT, H., MARKESTAD, P. & ØKLAND, D. 2001. Stress determination from hydraulic fracturing tests: the system stiffness approach. *International Journal of Rock Mechanics and Mining Sciences*, 38, 529-541.
- REYES, L. & OSISANYA, S. O. 2002. Empirical Correlation of Effective Stress Dependent Shale Rock Properties. *Journal of Canadian Petroleum Technology*.
- THORSEN, K. 2011. In situ stress estimation using borehole failures — Even for inclined stress tensor. *Journal of Petroleum Science and Engineering*, 79, 86-100.
- ZHANG, J., PORDEL SHAHRI, M., MISKA, S., MAJIDI, R., OZBAYOGLU, E. & YU, M. 2013. Modified Inversion Technique for Determining the In-situ Stress Field. Society of Petroleum Engineers.
- ZOBACK, M. D. & HAIMSON, B. C. 1982. Status Of The Hydraulic Fracturing Method For In-Situ Stress Measurements. American Rock Mechanics Association.

Appendix

This program is written by Segun G. Aiyeru as part of his MSc. thesis at the University of Stavanger, Norway. The program is to estimate the magnitude and direction of the horizontal in-situ stresses and predict fracture pressure based on the inversion method model proposed by Professor Bernt S. Aadnøy. The program is written for educational purposes and available for free to use. The writer will not be responsible for any damage, loss, expense or cost that may arise with the use of this program.

```

1. close all
2. clear all
3. clc
4. Excel_A = xlsread('C:\temp\Inv.xlsx');
5. Dataset = []; % Input the datasets combination to test
6. Prognosis_Datasets = []; % Input the test dataset as previous line + prognosis
7. nt = size(Prognosis_Datasets,2);
8. n = size(Dataset,2);
9. for i = 1:n
10. Pw(i) = Excel_A(Dataset(i),2);
11. Po(i) = Excel_A(Dataset(i),3);
12. Ov(i) = Excel_A(Dataset(i),4);
13. Inc(i) = Excel_A(Dataset(i),5);
14. Az(i) = Excel_A(Dataset(i),6);
15. end
16. rev = 1:91;
17. Beta = zeros(1,length(rev));
18. Sigma_1 =zeros(2,length(rev));
19. SQ_ER = zeros(1,length(rev));
20. Beta1 = zeros(1,length(rev));
21. Sig_both =zeros(2,length(rev));
22. squared_error = zeros(1,length(rev));
23. % Matrices Generation
24. for combi_nr=0:2^n-1 % START off all combinations
25. combination=num2str(dec2bin(combi_nr,n));
26. for i=1: n
27. if str2num(combination(i))==1
28. SIGDXY(i) =1;
29. else
30. SIGDXY(i)=0;
31. end
32. end
33. for j1 = 1:length(rev)
34. for k1 = 1:n
35. Azm1(j1,k1) = Az(k1)-(j1-1);

```

```

36. Beta1(1,j1) = (j1-1);
37. D1(j1,k1) = (sind(Azm1(j1,k1)))^2;
38. E1(j1,k1) = (cosd(Azm1(j1,k1)))^2;
39. F1(k1) = (sind(Inc(k1)))^2;
40. G1(k1) = (cosd(Inc(k1)))^2;
41. if SIGDXY(k1) == 0
42. A1(k1,1) = 3*D1(j1,k1)-E1(j1,k1)*G1(k1);
43. A1(k1,2) = 3*E1(j1,k1)-D1(j1,k1)*G1(k1);
44. Pp1(k1,1) = ((Pw(k1) + Po(k1))/Ov(k1)) + F1(k1);
45. else
46. A1(k1,1) = 3*E1(j1,k1)*G1(k1)-D1(j1,k1);
47. A1(k1,2) = 3*D1(j1,k1)*G1(k1)-E1(j1,k1);
48. Pp1(k1,1) = ((Pw(k1) + Po(k1))/Ov(k1)) - (3*F1(k1));
49. end
50. end
51. B1(1,k1) = A1(k1,1);
52. B1(2,k1) = A1(k1,2);
53. H1 = zeros(2,2);
54. for m1 = 1:n
55. % B*A
56. H1(1,1) = H1(1,1) + A1(m1,1)*A1(m1,1);
57. H1(1,2) = H1(1,2) + A1(m1,1)*A1(m1,2);
58. H1(2,1) = H1(2,1);
59. H1(2,2) = H1(2,2) + A1(m1,2)*A1(m1,2);
60. end
61. % Inverse of B*A
62. Det1 = H1(1,1)*H1(2,2) - H1(1,2)*H1(2,1);
63. T1(1,1) = H1(2,2)/Det1;
64. T1(1,2) = -H1(1,2)/Det1;
65. T1(2,1) = -H1(2,1)/Det1;
66. T1(2,2) = H1(1,1)/Det1;
67. Det1 = 0;
68. % Product of A transpose and Pp
69. S1 = zeros(2,1);
70. for q1 = 1:n
71. S1(1,1) = S1(1,1) + A1(q1,1)*Pp1(q1,1);
72. S1(2,1) = S1(2,1) + A1(q1,2)*Pp1(q1,1);
73. end
74. % Calculate stresses
75. Sig(1,1) = T1(1,1)*S1(1,1) + T1(1,2)*S1(2,1);
76. Sig(2,1) = T1(2,1)*S1(1,1) + T1(2,2)*S1(2,1);
77. Sig_both(:,j1) = Sig(:,1);
78. for z1 = 1:n
79. DXY1(j1,z1) = Sig(1,1)*(E1(j1,z1)*G1(z1) - D1(j1,z1)) +
    Sig(2,1)*(D1(j1,z1)*G1(z1) - E1(j1,z1)) + F1(z1);

```



```

80. end
81. % squared error
82. Datasetok = true;
83. for z1 = 1:n
84. if DXY1(j1,z1)< 0 && SIGDXY(z1)==0
85. Datasetok = false;
86. end
87. if DXY1(j1,z1)> 0 && SIGDXY(z1)==1
88. Datasetok = false;
89. end
90. end
91. err1 = (A1*Sig) - Pp1;
92. if Datasetok == true
93. squared_error(:,j1) = err1'*err1;
94. else
95. squared_error(:,j1) = 999;
96. end
97. squared_errorReal(:,j1) = err1'*err1;
98. end
99. error_sq_min = min(squared_error);
100. for bt1 = 1:length(rev)
101. if squared_error(1,bt1) == error_sq_min;
102. if Sig_both(1,bt1) < Sig_both(2,bt1)
103. Sig_1 = Sig_both(2,bt1);
104. Sig_2 = Sig_both(1,bt1);
105. Beta_angle = bt1-1+90;
106. else
107. Sig_1 = Sig_both(1,bt1);
108. Sig_2 = Sig_both(2,bt1);
109. Beta_angle = bt1-1;
110. end
111. end
112. end
113. % Testing the simulated results
114. for x = 1:n
115. New_Az(x) = Az(x)- Beta_angle;
116. D(x) = (sind(New_Az(x)))^2;
117. E(x) = (cosd(New_Az(x)))^2;
118. SigmaX(x) = (((Sig_1*E(x)) + (Sig_2*D(x)))*G1(x))+F1(x);
119. SigmaY(x) = (Sig_1*D(x)) + (Sig_2*E(x));
120. D_SigmaXY(x) = SigmaX(x) - SigmaY(x);
121. if D_SigmaXY(x)>0
122. Pwf_test(x) = (((3*SigmaY(x)) - SigmaX(x))*Ov(x))-Po(x);
123. else
124. Pwf_test(x) = (((3*SigmaX(x)) - SigmaY(x))*Ov(x))-Po(x);

```

```

125. end
126. end
127. %Error calculation on Pwf
128. for x = 1:n
129. errPwf(x)=Pw(x)-Pwf_test(x);
130. end
131. %save the result from all combinations
132. combinationsave(combi_nr+1,1:n)=SIGDXY;
133. estimatePwf(combi_nr+1,1:n)=Pwf_test;
134. sqrooterrPwf(combi_nr+1)=sqrt(errPwf*errPwf');
135. Sigresult(combi_nr+1,1)=max(Sig_1,Sig_2);
136. Sigresult(combi_nr+1,2)=min(Sig_1,Sig_2);
137. Sigresult(combi_nr+1,3)=Beta_angle;
138. Sigresult(combi_nr+1,4)=error_sq_min;
139. end % off all combinations
140. %print out the results
141. 'combinations'
142. combinationsave
143. 'Pwf_root_sqr_error'
144. sqrooterrPwf';
145. 'sHmax, shmin, beta, sHh_error'
146. Sigresult
147. 'Final result'
148. minerrComb=find(sqrooterrPwf==min(sqrooterrPwf)); % find minimum indices
149. if minerrComb<999 % there was some legal results found
150. 'Best combination'
151. minerrComb
152. combinationsave(minerrComb,1:n)
153. 'Estimated Fracture Pressure'
154. estimatePwf(minerrComb,1:n)
155. Final_estimatePwf = estimatePwf(minerrComb,1:n);
156. 'Pwf error'
157. sqrooterrPwf(minerrComb)
158. 'sHmax, shmin, beta, sHh_error'
159. Sigresult(minerrComb,1:4)
160. Final_sigma1 = Sigresult(minerrComb,1);
161. Final_sigma2 = Sigresult(minerrComb,2);
162. Final_beta = Sigresult(minerrComb,3);
163. else
164. 'No good solution was found'
165. end
166. % Prognosis for future well
167. for i = 1:nt
168. Pw2(i) = Excel_A(Prognosis_Datasets(i),2);
169. Po2(i) = Excel_A(Prognosis_Datasets(i),3);

```

In-Situ stress measurement from LOT data using Inversion method

```
170. Ov2(i) = Excel_A(Prognosis_Datasets(i),4);
171. Inc2(i) = Excel_A(Prognosis_Datasets(i),5);
172. Az2(i) = Excel_A(Prognosis_Datasets(i),6);
173. end
174. for sd = 1:nt
175. if Pw2(sd)==0
176. New_Az2(sd) = Az2(sd)- Final_beta;
177. D2(sd) = (sind(New_Az2(sd)))^2;
178. E2(sd) = (cosd(New_Az2(sd)))^2;
179. F2(sd) = (sind(Inc2(sd)))^2;
180. G2(sd) = (cosd(Inc2(sd)))^2;
181. SigmaX2(sd) = (((Final_sigma1*E2(sd)) + (Final_sigma2*D2(sd)))*G2(sd))+F2(sd);
182. SigmaY2(sd) = (Final_sigma1*D2(sd)) + (Final_sigma2*E2(sd));
183. D_SigmaXY2(sd) = SigmaX2(sd) - SigmaY2(sd);
184. if D_SigmaXY2(sd)>0
185. Pwf_test2(sd) = ((3*SigmaY2(sd)) - SigmaX2(sd))*Ov2(sd)-Po2(sd);
186. else
187. Pwf_test2(sd) = ((3*SigmaX2(sd)) - SigmaY2(sd))*Ov2(sd)-Po2(sd);
188. end
189. else
190. Pwf_test2(sd) = Final_estimatePwf(sd);
191. end
192. end
193. 'Estimated with Prognosed Fracture Pressure'
194. Pwf_test2
```